Spatio-temporal variability of ocean currents at the Amundsen Sea shelf break and their link to CDW inflow and ice-shelf melt

Alban Planchat[1,2], Nicolas C. Jourdain[1], Pierre Dutrieux[3]

[1]Université Grenoble Alpes/CNRS/IRD/G-INP, IGE, Grenoble, France
[2]LMD-IPSL, École Normale Supérieure/PSL University, CNRS, École Polytechnique, Sorbonne Université, Paris, France
[3]British Antarctic Survey, Cambridge, UK

Key Points:

- A Fresh-Warm Boundary Index (FWBI), based on sea surface height, is created to follow the evolution of the fresh-warm shelves limit
- The ocean interannual-to-decadal variability at the shelf break, especially in Russel Bay, is connected with ice-shelf melt variability
- El Niño-Southern Oscillation has no strong correlation with the ice-shelf basal melt variability, except for the very recent years

Corresponding author: Alban Planchat, `alban.planchat@orange.fr`

Abstract

Understanding the driving processes at stake for the Circumpolar Deep Water (CDW) intrusion onto the Amundsen shelf is crucial. We use a multi-decadal ocean simulation at 1/12° to revisit the ocean dynamics at the Amundsen shelf break, distinguishing a western fresh shelf and an eastern warm shelf. While the prevailing presence of the Antarctic Slope Current - fed to the east of Russel Bay through vortex stretching of an outflow of melted waters - blocks CDW intrusions in the west, the contact of Antarctic Circumpolar Current (ACC) branches along the shelf in the east favors this inflow. Of particular importance is a southern ACC branch initiated to the south-east of the Ross Gyre, which interacts with the topography at the entry of the western Pine Island-Thwaites trough. Then, we link the ocean interannual-to-decadal variability at the shelf break with the ice-shelf basal melting and create a Fresh-Warm Boundary Index (FWBI) to follow the oscillation of the fresh-warm shelves limit through time in Russel Bay, which could be a focal point to understand the low frequency fluctuations of the basal melt. We suggest that not only a wind-induced Ekman pumping could favor the CDW inflow at the shelf break, but also topographic interactions, a bottom Ekman transport, a sea-ice–induced Ekman pumping resulting from strong surface currents, and the baroclinicity of the eastward along-shelf current in the west. Finally, we highlight that El Niño-Southern Oscillation has no strong correlation with the ice-shelf basal melt variability, except for the very recent years.

Plain Language Summary

The Amundsen Sea ice sheet has been experiencing the highest mass loss around Antarctica. The complex interaction between the ocean and the ice sheet in the region due to the onshelf accumulation near the ice-shelf grounding line of relatively warm and salty water found at depth around Antarctica is thought to have triggered this mass loss. In order to understand the observed interannual-to-decadal variability of the ice-shelf basal melt, we use a high resolution multi-decadal simulation to revisit the ocean dynamics at the Amundsen shelf break, distinguishing two types of shelves that we characterize in depth. Then, we link the ocean low frequency fluctuations at the shelf break with the ice-shelf basal melt, and an index, also potentially producible from satellite altimetry, is created to follow the fresh-warm shelves limit through time in Russel Bay. In particular, this bay located along the shelf break, could be a focal point to understand the interannual-to-decadal variability of the basal melt. Finally, after suggesting mechanisms for the warm and salty water inflow at the shelf break, we highlight that El Niño-Southern Oscillation (ENSO) has no strong correlation with the ice-shelf basal melt variability, except for the very recent years.

1 Introduction

The Antarctic Ice Sheet (AIS) mass loss has been increasing over the past four decades, from about 40 Gt.yr^{-1} in the 1980s to roughly 250 Gt.yr^{-1} in the 2010s (Rignot et al., 2019). This mass loss signal is dominated by the West Antarctic Ice Sheet (WAIS), and in particular the Amundsen Sea sector where ice thinning and grounding line retreat have been reported (Mouginot et al., 2014). The single contribution of Pine Island Glacier has reached 3.0 mm of global mean sea level rise between 1979 and 2017, which is almost as much as the entire contribution of the East Antarctic Ice Sheet over the same period (Rignot et al., 2019). Therefore, there is a growing demand to understand the complex interactions between the atmosphere, the ocean and the ice sheet in the Amundsen Sea Embayment (Pörtner et al., 2019).

The changes in WAIS mass loss have been attributed to increased intrusion of relatively warm and salty Circumpolar Deep Water (CDW) onto the continental shelf (e.g., Jacobs et al., 2013). These intrusions mostly occur through a cyclonic circulation in the bathymetric troughs joining the shelf break and the ice-shelves (Assmann et al., 2013; Dotto et al., 2019). They are favored by wind-induced anomalies of heat transport across the continental shelf break of the Amundsen Sea, located at the limit between the westerlies – blowing over the deep Southern Ocean – and the easterlies – blowing along the AIS margin – (Thoma et al., 2008; Steig et al., 2012; Webber et al., 2017; Kimura et al., 2017; Holland et al., 2019). Other processes occuring at the shelf break and mediating a heat transport towards the Amundsen shelf have been reported: the effect of bottom Ekman transport (Wåhlin et al., 2012) to mesoscale eddies at the shelf break (St-Laurent et al., 2013; Stewart & Thompson, 2015), the role of advection (Rodriguez et al., 2016), or the consequence of the seasonal sea ice drift (Kim et al., 2017) and temperature anomalies associated to coastal-trapped Kelvin waves (Spence et al., 2017). In addition, the retrograde seabed slope, mostly deepening from the shelf break to the ice-shelves (Figure 1), favors the formation of a warm pool near the ice-shelf grounding lines. Thus, moderate ocean warming may induce tipping points with an irreversible ice sheet instability in the region (Rosier et al., 2020).

The Amundsen Sea was proposed to be located at a transition between a fresh shelf along the eastern Ross Sea and a warm shelf along the Bellingshausen Sea (Thompson et al., 2018; Moorman et al., 2020). A fresh shelf is characterized by a positive sea surface height (SSH) anomaly over the continental shelf, induced by easterly winds and favoring the westward Antarctic Slope Current (ASC) near the ocean surface, blocking cross-shelf exchanges and keeping the shelf sub-surface waters relatively cold. In contrast, a warm shelf is characterized by the quasi absence of ASC, relatively warm sub-surface shelf waters and significant cross-shelf exchanges (Thompson et al., 2018). At a few hundreds of meters depth, the density structure near the shelf break of the Amundsen Sea sometimes induces an eastward "undercurrent" which favors CDW inflows into the aforementionned bathymetric troughs (Walker et al., 2013; Assmann et al., 2013). The Amundsen Sea may also be impacted by the eastern flank of the cyclonic Ross Gyre and by multiple unsteady branches of the eastward Antarctic Circumpolar Current (ACC) (Orsi et al., 1995; Walker et al., 2013; Thompson et al., 2018; Nakayama et al., 2018).

This modelling study is part of a collective effort to improve models to better represent the processes at stake in the Amundsen Sea and their interactions so as to enhance our understanding of the driving mechanisms for CDW inflow and their effect on ice-shelves melt (e.g., Pörtner et al., 2019; Dotto et al., 2019, 2020; Jourdain et al., 2017, 2019; Kimura et al., 2017; Nakayama et al., 2014, 2018). Especially, how the transition between fresh and warm shelves varies in time and how this affects ice-shelf melting has not been comprehensively addressed so far in the region (Moorman et al., 2020; Dotto et al., 2019). In this paper, we revisit the ocean circulation at the shelf break throughout the Amundsen Sea using a multi-decadal ocean simulation accounting for tides and ocean-ice-shelves interactions.

2 Material and Methods

2.1 Simulation

We use the Nucleus for European Modelling of the Ocean (NEMO-3.6, Madec (2016)) that includes the general oceanic circulation model, *Océan Parallélisé* (OPA) and the Louvain-la-Neuve sea Ice Model (LIM-3.6, Rousset et al. (2015)). Our model set-up includes the representation of ocean–ice-shelf thermodynamical interactions (Mathiot et al., 2017). In particular, the configuration is similar to Jourdain et al. (2017, 2019) except that the domain, named AMUXL, was slightly extended westard as well as eastward, and that we use interannual forcing. The new domain extends from 142.0°W to 85.0°W and from 76.3°S to 59.8°S.

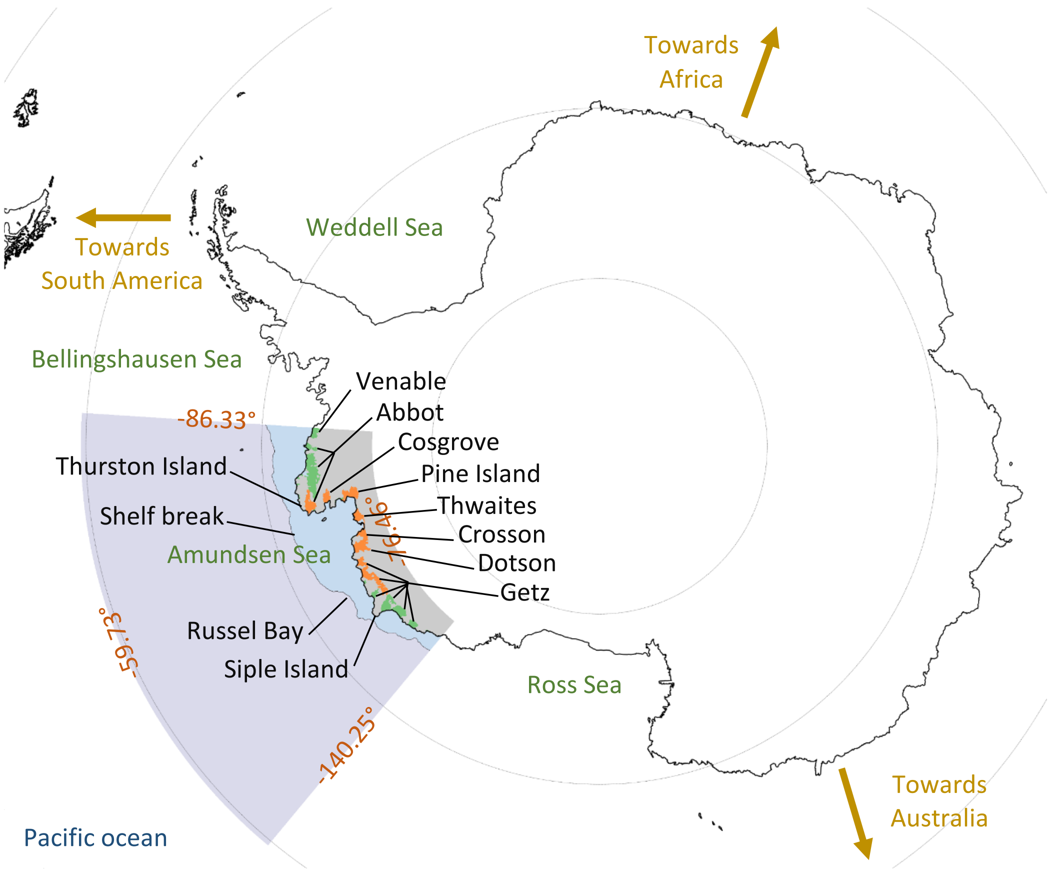

Figure 1. Studied area. The shaded zone in the western part of Antarctica corresponds to the simulated region. It covers the entire Amundsen Sea, slightly outflanking towards the Ross Sea to the west and towards the Bellingshausen Sea to the east. The limit between the deep ocean (light purple) and the shelf (light blue) is represented with a grey continuous line at the shelf break as defined in section 2.2. The main ice-shelves of the region are colored either in orange for those part of the Amundsen Sea and in green for the others. In the analysis, we refer many times to Russell Bay, which is located between 128°W and 124°W.

The model is run with 75 vertical levels ranging from 1m thickness at the surface to 204 m at 6000 m, with the highest and deepest ocean cell having a thickness adapted to match the ice-shelf draft and bathymetry, respectively. The horizontal grid is quasi-isotropic, with 1/12° resolution in longitude, i.e., from 4.7 km at the northern boundary to 2.2 km in the southernmost part of the domain, and a resolution between 2.5 and 3.5 km over the continental shelf. This resolution enables to partly resolve meso-scale eddies offshore, but not on the continental shelf. According to St-Laurent et al. (2013) and Stewart and Thompson (2015), such a resolution enables to correctly resolve the mean flow-topography interaction inside the troughs on the shelf, but it cannot resolve the wave-topography interaction.

The ice-shelf and seabed topography is extracted from v1.33 of BedMachine-Antarctica (Morlighem et al., 2020). That version contained an error in geoid height for the IBCSO bathymetry, so that our ocean bathymetry is too shallow, with an error increasing from 15 to 55 m eastward across our domain. Our simulation runs from March 1972 to December 2018, and we use 1972-1979 to spin up the model, i.e., we only analyze results from January 1980. The simulation is driven by the Drakkar Forcing Set (DFS5, Dussin et al., 2016) based on ERAinterim (Dee et al., 2011) from 1979 and ERA40 (Uppala et al., 2005) before that. As DFS5 ends in 2015, we use uncorrected ERAinterim outputs from 2016 to 2018. The lateral ocean and sea ice boundary conditions comes from a global NEMO simulation that has the exact same characteristics as the one used by Merino et al. (2018), except that it has a longer spin up, and that the imposed ice-shelf melt flux increases linearly from 1990 to 2005 and is constant before and after that, with values corresponding to the FRESH+ and FRESH− reconstructions of Merino et al. (2018). The freshwater released by melting icebergs is calculated through a Lagrangian iceberg model (Marsh et al., 2015; Merino et al., 2016) in the global NEMO simulation used as lateral boundary conditions, and re-injected as a monthly surface flux in our regional simulation. Barotropic tide is prescribed from seven constituents of FES2012 (Carrère et al., 2012; Lyard et al., 2006) at our domain boundaries, as in Jourdain et al. (2019).

Some parameter values are summarized in Tab. 1 and the complete list of parameters can be found on `https://doi.org/10.5281/zenodo.5521569`. An evaluation of our simulation is presented in Appendix Appendix A. Our main findings are that (*i*) our simulation underestimates the sea ice extent by about 16 % on average but the interannual variability of the maximum sea ice extent is well captured by our model; (*ii*) our simulation tends to slightly overestimate the ice-shelf basal melt rates with, for instance, a 10 % overestimation for Pine Island, but the range of values in between the ice-shelves is well represented; (*iii*) our simulation has a warm bias throughout the water column on the Amundsen continental shelf, but it does not exceed 0.5 °C. Despite such biases, the mean circulation, its gradients, and the range of variability observed on the shelf seas are consistent with the observations. In the following, we assume the model is an acceptable representation of reality.

2.2 Shelf Break Reference Frame

We now present a method to visualize the ocean dynamics and properties along the continental shelf break. First, it requires to properly identify the break, at the edge between the continental shelf and the continental slope. Then, we define the along shelf break and orthogonal directions used throughout our paper.

The continental shelf break is often poorly defined. In the Amundsen region, it is generally simply considered as an isobath line, most of the time between 700 and 1500 m depth. However, such a delineation of the shelf break omits the irregularity of its depth, especially due to the initiation of the on-shelf submarine troughs.

Table 1. Model parameters to describe ocean interfaces.

Parameter	Value (unitless)	Description
$C_D{}^{iw}$	5.00×10^{-3}	Ocean–sea-ice drag coefficient
$C_D{}^{ai}$	1.40×10^{-3}	Air–sea-ice drag coefficient
$C_D{}^{aw}$	Wind-dependent	Air–ocean drag coefficient
C_D	1.00×10^{-3}	Ocean–ice-shelf drag coefficient
Γ_T	2.21×10^{-2}	Ocean–ice-shelf heat exchange coefficient (Stanton number $St_T = \sqrt{C_d}\Gamma_T = 0.0007$)
Γ_S	6.19×10^{-4}	Ocean–ice-shelf salt exchange coefficient

We first develop a shelf-break delineation method in a way to identify the upper part of the shelf break while clearly distinguishing it from other bathymetric features on the continental shelf. It consists of the two following steps:

1. We identify the location of the 773 m isobath since a shallower one poses problems near Siple Island (see location in Figure 1);
2. We translate southward each point of this line until it reaches a bathymetric slope threshold of 0.0125 (i.e., 12.5 m vertically per horizontal kilometer; calculated as the norm of the slope vector averaged in the eight surrounding grid directions).

The resulting shelf break line is plotted in Figure 2a. Such a delineation enables the representation of the submarine troughs as illustrated by the bathymetry along the shelf break, displayed Figure 2b. The method that is presented here could be applied to other regions, although the isobath and slope thresholds may need to be adjusted.

We then create a new reference frame, which corresponds to the along-break and orthogonal directions at each point of the shelf break line. To avoid misleading projections in the new reference frame due to the curvature of some bays in the region along the shelf break (e.g., Russel Bay, Figure 1), we manually create shortcuts of the shelf break line (see dashed line in Figure 2a). This shortcut line is used to define the along-break and orthogonal directions offshore of this line (purple segments in Figure 2a), while the original shelf break delineation is used to calculate these directions on the continental shelf and in the large bays (green segments in Figure 2a). The origin of each local rotated frame remains the original shelf break line, and all relevant ocean quantities can be interpolated onto the rotated frames all along the shelf break. Finally, we plot many results as a function of the along-break distance which is defined from the westernmost point of our domain.

This new reference frame should be considered as the juxtaposition of near-orthogonal transects to the shelf break. Note that for more readability of the figures, the (Ox') (resp. (Oy')) axis will be referenced as "Along shelf break distance (km)" (resp. "Orthogonal distance (km)", even though it is near-orthogonal). Similarly, x (resp. y) is used in the text to refer to the along (resp. cross) shelf break distances. Finally, as the shelf break is mostly zonal, we abusively call the rotated directions eastward, westward, southward and northward directions although the shelf break is not exactly aligned with a parallel.

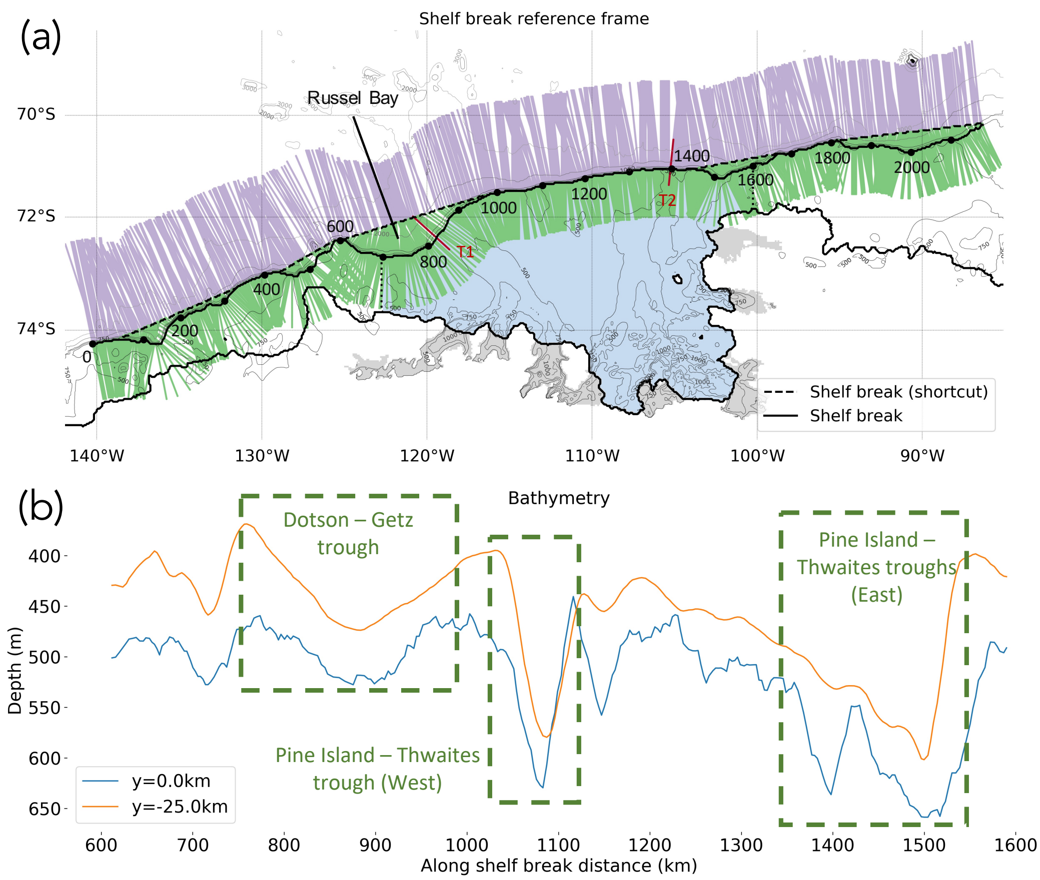

Figure 2. Method used to delineate the shelf break and to define near-orthogonal transects (see section 2.2). (**a**) The black lines represent the ice sheet margin and continental shelf break (solid lines) and the shelf break shortcut (dashed line) used to determine the offshore direction. The green and purple segments refer to the near-orthogonal direction at every point of the shelf break line. The along shelf break distances (from the western domain boundary) are indicated every 100km. The T1 and T2 red lines are the two cross-sections used in Figure 4 to show the Dotson-Getz trough and the eastern Pine Island-Thwaites trough. The ice-shelves of interest (from the eastern part of Getz to Cosgrove) are colored in grey. The blue area shows the continental shelf area used in Figure 11, and is delineated by the ice sheet margin to the south, the shelf break line to the north and the dotted lines to the west and east. (**b**) shows the bathymetry along the shelf break (blue line) and 25 km further inshore onto the continental shelf (orange line). The green boxes indicate the major bathymetric troughs.

3 Results

We first analyze the mean ocean state along the Amundsen shelf break allowing us to distinguish, on average, both a fresh and a warm shelf in the region according to the definition given by Thompson et al. (2018). We describe the multiple currents observed along the shelf break, then we analyze their variability in connection with the ice-shelf basal melt interannual-to-decadal fluctuations. Even though the model domain covers a larger area than the Amundsen Sea in the west and in the east, we only present results, and discuss them, for the Amundsen region.

3.1 Fresh Versus Warm Shelves

Considering the mean state of the ocean between 1980 and 2018, we can make a distinction between a western fresh shelf and an eastern warm shelf in the region.

Indeed, in the western part of the Amundsen Sea, the thermocline is relatively deep compared to the east (Figure 3d,e). The ocean conservative temperature (CT) at 301 m depth at the shelf break is negative in the western part versus positive in the eastern part of the Amundsen Sea (Figure 3a), which indicates a transition from a fresh to a warm shelf (see Section 1). The same distribution is observed for the absolute salinity (AS) with saltier waters at 301 m depth at the shelf break in the eastern Amundsen Sea (not shown). These relatively warm and salty waters indicate the presence of CDW closer to the surface in the warm shelf region.

The distinction between a western fresh shelf and an eastern warm shelf is also apparent looking at the near-surface current aligned with the shelf break for y∈[0, 50] km (Figure 3b). A westward current is present just off the shelf break in the western Amundsen Sea, which corresponds to the ASC, and is typical of fresh shelves. In contrast, an eastward current is observed in the eastern Amundsen Sea, which corresponds to an ACC branch, with meanders (e.g., near x=1500 km and x=1850 km) associated with bathymetric features. As previously reported, the ASC has a baroclinic structure on average, shearing eastward with increasing depth, while the eastward current in the eastern region appears to be rather barotropic on average (Figure 3b,c). The transition between the two types of shelves is located at the western extremity of Russell Bay (see location in Figure 1).

Typical cross-sections at the shelf break for both types of shelves are displayed in Figure 4. T1, being located at the entry of the Dotson-Getz (Do-Ge) trough at x=826 km, is used as an example of a fresh shelf cross-section, whereas T2, being located at the entry of the eastern Pine Island-Thwaites (Pi-Th) troughs at x=1398 km (left one), is an example of a warm shelf cross-section. Additional cross-sections in between the Do-Ge trough and the western PI-Th trough are presented in supplementary (Appendix Appendix B).

The CT cross-sections (Figure 4a,b) highlight the presence of CDW onto the continental shelf in the warm shelf zone although the vertical shift between a negative CT and a positive CT happens at the same isopycnal (~27.55 kg/m^3). This is due to both the shallower seafloor in the western Amundsen Sea at the shelf break and to the deeper ~27.55 kg/m^3 isopycnal associated with the prevailing presence of the ASC in the upper ocean layer just off the shelf in the west (Figure 3b) - blocking the warm and salty CDW at the shelf break in the fresh shelf zone.

Four different currents can be spotted on these cross-sections (Figure 4c,d). For y∈[0, 50] km the ASC is visible on the fresh shelf cross-section (T1) in the upper part of the water column, as well as the ACC branch over the entire water column for the warm shelf cross-section (T2). An eastward current is visible on both cross-sections at the limit of the shelf break (-20<y<10 km). The eastward flow appearing on T1 for y>50 km is

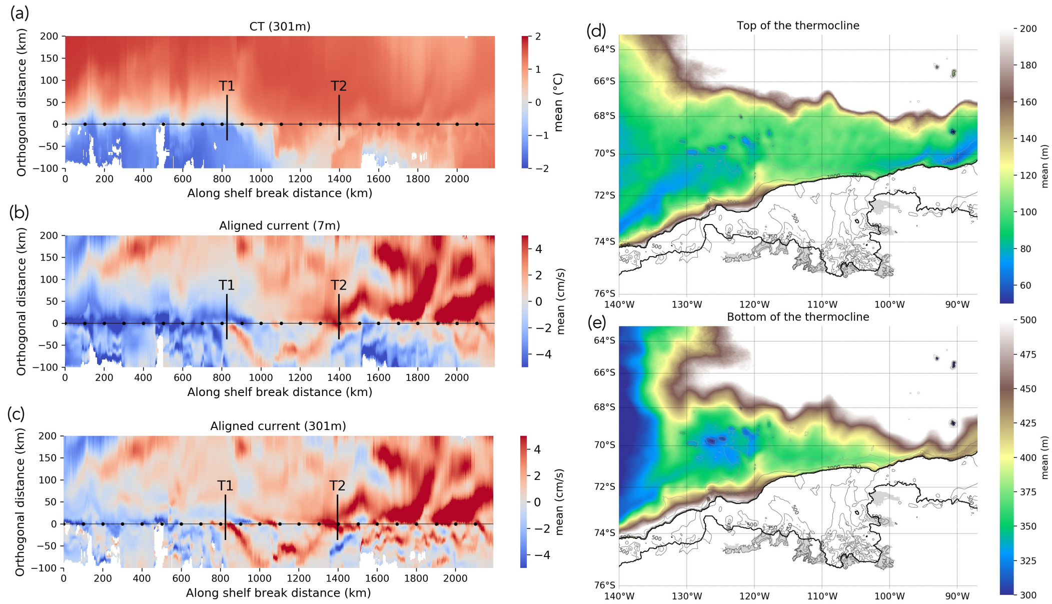

Figure 3. Mean ocean state. (**a**), (**b**) and (**c**) respectively show the mean CT at 301 m and the mean aligned current at 7 and 301 m. The black continuous line at y=0 km corresponds to the shelf break with markers every 100 km. The cross-sections T1 and T2 (see location in Figure 2) used on Figure 4 are also drawn. (**d**) and (**e**) show the mean thermocline top and bottom depths off the Amundsen shelf, which is delineated with a black continuous line. The top and bottom thermocline depths are defined by looking for the shallowest and deepest depths where the vertical CT gradient is negative (z upward) and stronger than a -0.002 °C.m^{-1} threshold.

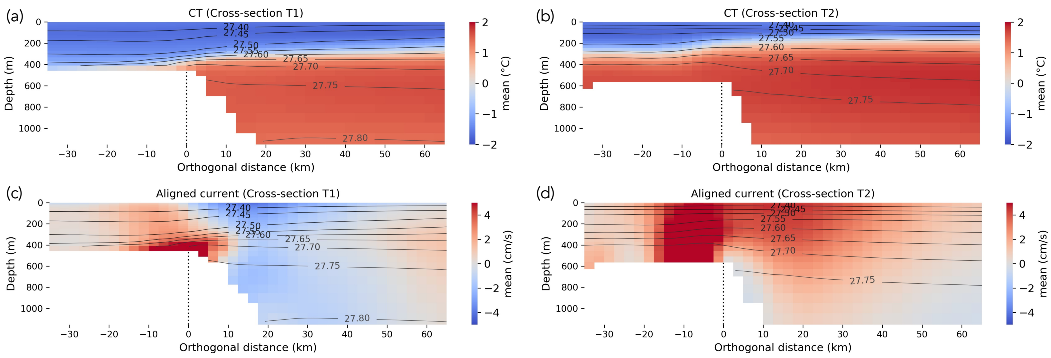

Figure 4. Cross-sections climatologies of CT (**a**, **b**) and the along-shelf ocean velocity (**c**, **d**) for T1 (left panels) and T2 (right panels) (see location in Figure 2). In panels (**c**) and (**d**), a red (resp. blue) color means that the current is globally eastward (resp. westward). Isopycnals (potential density anomalies) are plotted every 0.05 kg.m^{-3} and the identified shelf break is shown as a dotted black line at y=0 km.

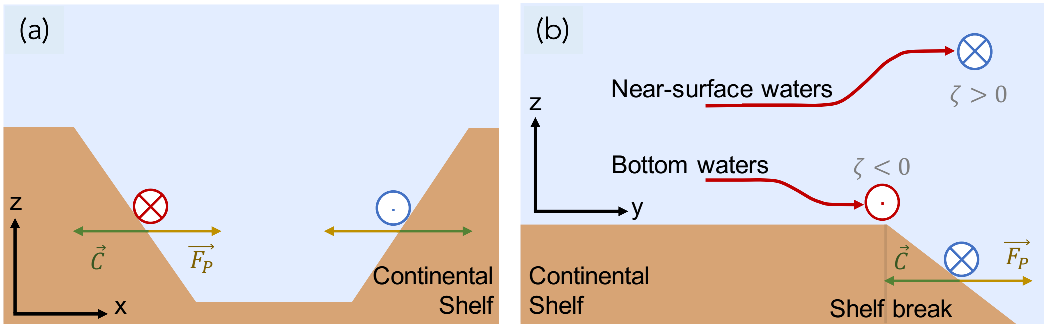

Figure 5. Schematic of some currents mechanisms. (**a**) is a schematic of the cyclonic circulation within a trough illustrated by a simple geostrophic balance. (**b**) is a suggestion for the schematization of the two distinct cases encountered for on-shelf currents reaching the shelf break depending on their depth. On (**a**) and (**b**), the currents are displayed in red (resp. blue) whether they are northward or eastward (resp. southward or westward). $\vec{C}$ refers to the Coriolis force and $\vec{F_P}$ to the pressure force.

an ACC branch located further offshore that is discussed later in this paper. Finally, a westward undercurrent is found along the continental slope of both shelves, but with a much smaller amplitude and extension in the case of T2. In the remaining part of this section, we describe these currents in more details and discuss their dynamical origin.

We first focus on the eastward current at the extremity of the continental shelf (-20<y<10 km), which is often referenced to as the eastward "undercurrent". We report differences in vertical structure and shape between the two types of shelf. While the current is very barotropic for the warm shelf (confusing with its "undercurrent" qualification), it appears to be more baroclinic and to extend further towards the continental slope at depth for the fresh shelf. This extension at depth, below the ASC, is consistent with the positive meridional density gradient at depth at the shelf break in the fresh shelf zone - as opposed to the negative meridional density gradient in the warm shelf zone - (see isopycnals in Figure 4c,d), allowing for an eastward geostrophic shear and a reversal of the surface current with depth (Thompson et al., 2018). With regards to the initiation of this eastward current along the shelf break, on the one hand, we suggest for the one at the entry of the Do-Ge trough that the return current - associated with the cyclonic circulation inside the trough - experiences a vortex stretching due to the isopycnals at depth. This leads, through potential vorticity (PV) conservation, to a cyclonic rotation, inducing an eastward turn of this water mass at the shelf break (Figures 4c and 5b). On the other hand, in the case of the eastern Pi-Th trough, we suggest that the eastward undercurrent is essentially generated in the western Pi-Th trough through topographic interactions with an ACC branch (see Section 4.1).

The initiation of the ASC coincides with an important outflow located in the upper half of the water column, between the eastern flank of the Do-Ge trough and the western flank of the western Pi-Th trough, which was reported by Walker et al. (2013, their Figure 7) and can be spotted on the bottom panel of the movie "Aligned_current_Oxz_Oxy.mp4" in supplementary (Appendix C1). The ASC is mainly composed of a near-surface fresh water mass that is compressed following the upsloping isopycnals at the shelf break. The PV conservation hence leads to an anticyclonic rotation, inducing a westward turn of this water mass at the shelf break (Figure 5b).

The bathymetry also plays an important role in shaping the currents. The pressure gradient exerted by a bathymetric slope makes geostrophic currents keep the bathy-

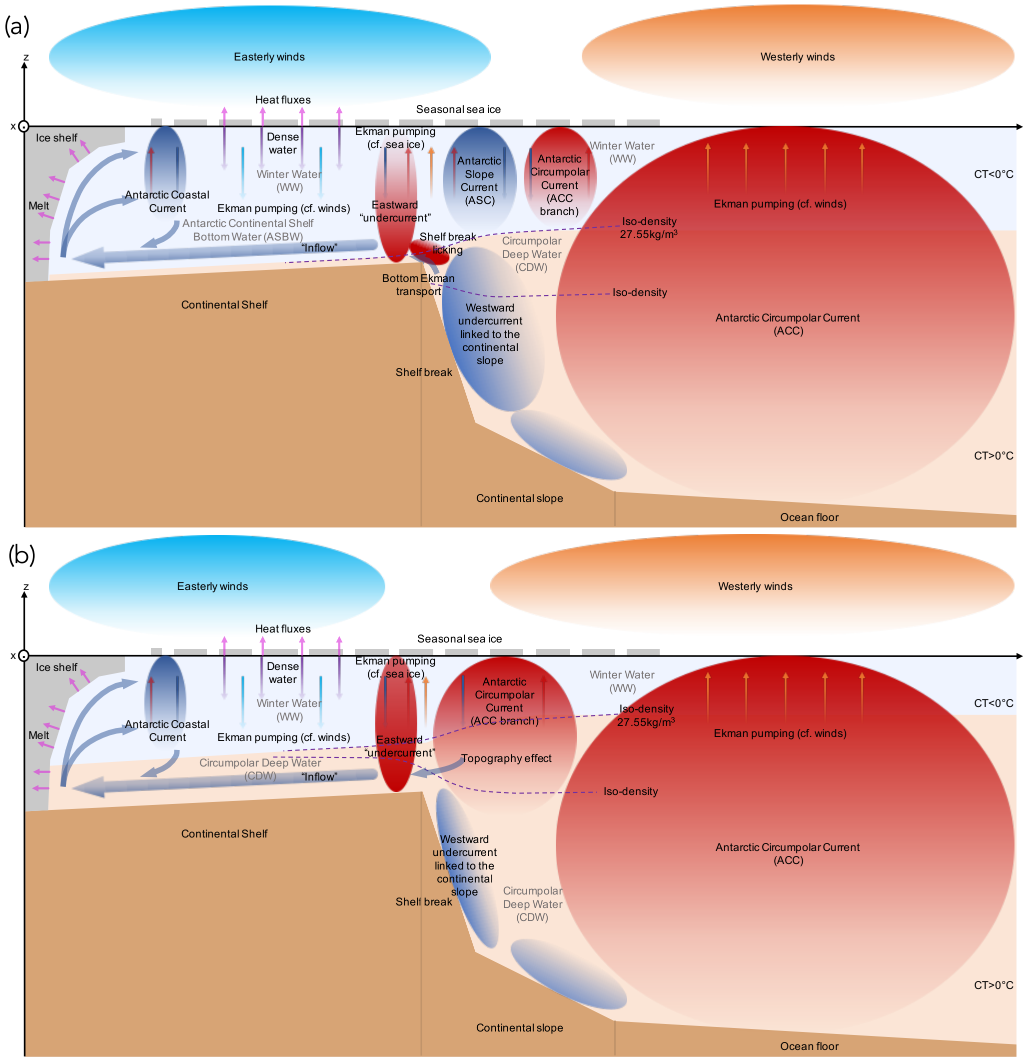

Figure 6. Schematic of the ocean state across the mean fresh (**a**) and warm (**b**) shelves in the Amundsen Sea. Note that the color of the currents refers to their orientation. A red (resp. blue) color means that the current is globally eastward or northward (resp. westward or southward)

metric slope to their left (Figure 5a), and the PV conservation makes them flow along isobaths (see also St-Laurent et al. (2013)). The geostrophic balance resulting from the bathymetric slope could also explain the presence of a westward undercurrent just over the continental slope for both types of shelf (Figures 4c,d and 5b) as well as the negative meridional density gradient along the continental slope allowing for a westward geostrophic shear.

The position of the typical currents at fresh and warm shelves is schematized in Figure 6.

3.2 Variability at the Shelf Break

The presence of both a fresh and a warm shelf in the Amundsen Sea is robust over time, but there is some variability that we now describe.

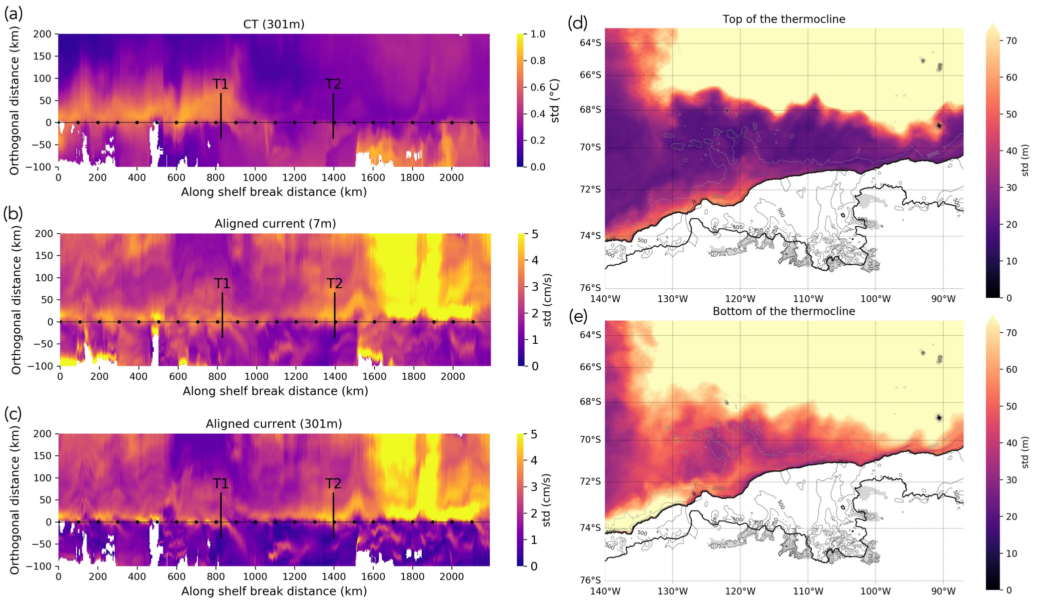

Figure 7. Standard deviation of the ocean dynamics and properties at the shelf break (see corresponding mean state in Figure 3). (**a**), (**b**) and (**c**) show the standard deviation of the CT at 301 m and the aligned current at 7 and 301 m, respectively. The black solid line at y=0 km corresponds to the shelf break with markers every 100 km. The cross-sections T1 and T2 (location shown in Figure 2) used in Figure 4 are also drawn. (**d**) and (**e**) show the standard deviation of the thermocline top and bottom depths off the Amundsen shelf, which is delineated with a black solid line.

The depths of the upper and lower thermocline have a larger variability along the shelf break in the fresh shelf zone than in the warm shelf zone (Figure 7d,e). This is consistent with the ASC variability (Figure 7b,c), as a stronger ASC pushes the thermocline deeper and blocks intrusions of CDW onto the shelf. The surface current just off the fresh shelf (ASC in the mean state) sometimes switches from westward to eastward, and the reverse is observed in the warm shelf region as shown on the top left panels of the "Aligned_current_T1_T2.mp4" movie in supplementary (Appendix C2). This shows that the southern ACC branch can be intermittently stuck at the shelf break further to the west, and that the ASC can sometimes be initiated further to the Bellingshausen Sea - as proposed by Thompson et al. (2020). These two types of intermittent events can be observed on the two panels of the "Aligned_current_Oxz_Oxy.mp4" movie in supplementary (Appendix C2). In particular, on the bottom panel, we observe that when a southern ACC branch gets in contact with the shelf break near Siple Island, to the west of Russel Bay, the eastward "undercurrent" at the entry of the Do-Ge trough has a higher magnitude (bottom panel). We infer from these intermittent events that, even though the Do-Ge trough is part of the fresh shelf zone on average, it can intermittently experience an interaction with a southern ACC branch - which could enhance CDW intrusions onto the shelf. The role of this specific southern ACC branch is discussed in Section 4.1.

The aligned current just off the continental shelf (y∈[0, 25] km) exhibits a high frequency variability with variations that appear almost instantaneously all along the shelf break (vertical stripes in Figure 8b). In contrast, CT at 301 m shows variability at a lower frequency (Figure 8a). CT anomalies seem to be initiated in the sector x∈[600, 1000] km, which corresponds to Russell Bay. These anomalies then propagate both eastward and

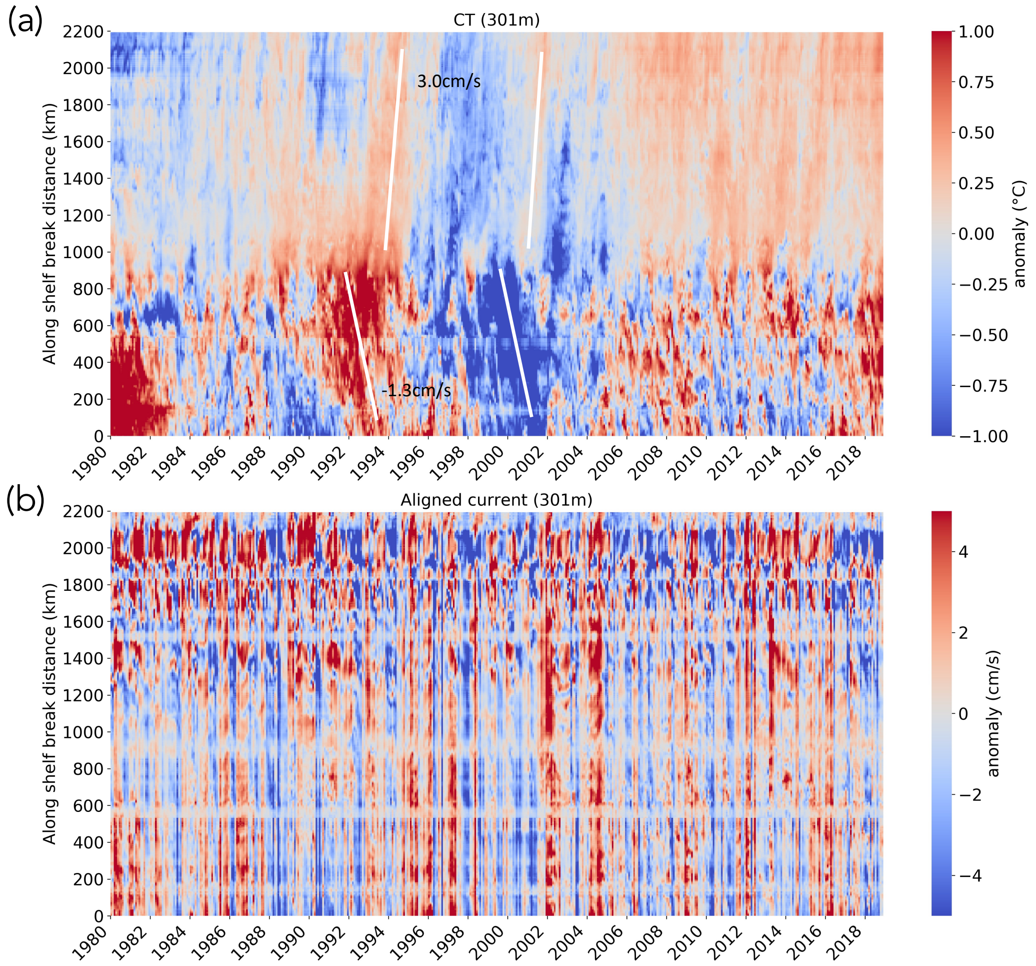

Figure 8. Variabilities at the shelf break. Hovmöller diagrams of the CT anomaly at 301 m (**a**) and the aligned current at 301 m (**b**) averaged between y=0 and y=25 km all along the shelf break. Note that a red (resp. blue) aligned current anomaly means that the current is globally more eastward (resp. westward) compared to the mean.

westward at speeds of 3.0 cm.s^{-1} and -1.3 cm.s^{-1}, respectively. This seems to be in adequation with the CT advection associated with the aligned current just off the shelf break (ACC in the east and ASC in the west). This result highlights the importance of understanding the key processes occurring at Russell Bay, which, in average, is the limit between the fresh and warm shelves. Regarding the aligned speed anomalies, the vertical bands suggest coastal-trapped Kelvin waves that could be initiated further to the east of the Amundsen Sea (Spence et al., 2017).

Given that some variability seems to emerge from the boundary between the fresh and warm shelves, we now define an index to follow variations in the location of this boundary. As it would be potentially useful to have an observational equivalent, we define this index based on SSH gradients, which are observed through satellite altimetry and are directly related to surface currents. The reversal of the surface currents between the fresh and warm shelves (ASC versus ACC branch) is indeed consistent with a reversal of the SSH gradient orthogonal to the shelf break.

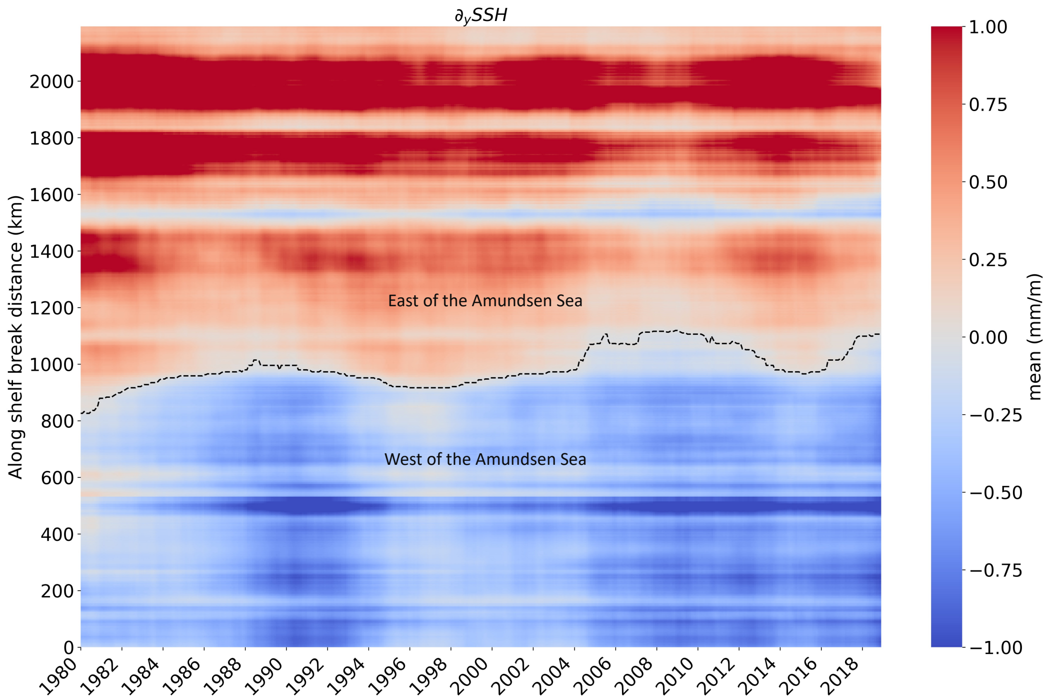

Figure 9. Evolution of the fresh-warm boundary. Hovmöller diagram of the SSH gradient orthogonal to the shelf break, with a 5-year running mean and averaged for y∈[0, 25] km for each point along the shelf break. The dashed black line shows the Fresh-Warm Boundary Index (FWBI).

The Fresh-Warm Boundary Index (FWBI) is defined as the along–shelf-break distance at which the SSH orthogonal gradient just off the shelf reverses - being negative in the west (ASC) and positive in the east (ACC). It oscillates between 800 and 1100 km at decadal scales over the 1980-2018 period (Figure 9 and discussed in Section 3.3), with a trend corresponding to an eastward drift towards the entry of the Pi-Th western trough. Note that the FWBI was built with a 5-year running mean, in agreement with the objective to study the interannual-to-decadal variability of the ice-shelf basal melt.

Finally, the eastward "undercurrent" also presents a variability. Indeed, as shown on the "Aligned_current_T1_T2.mp4" movie in supplementary (Appendix C2), the baroclinic component stays relatively stable through time - being very marked at depth at the entry of the Do-Ge trough (T1) and almost absent at the entry of the Pi-Th trough (T2) -, while the barotropic component varies in magnitude.

3.3 Connections with ice-shelf basal melt

We now analyze the relationships between the variability at the shelf break and the ice-shelf basal melt.

The characteristics and the basal melt rates of the seven ice-shelves of interest in the region are shown in Figure 10a,b. In the following, we only consider the eastern part of Getz and the western part of Abbot to only focus on the Amundsen Sea. As described in Appendix Appendix A, the mean ice-shelf basal melt rates found in our simulation are globally in the range of the observed values reported by Rignot et al. (2013), Depoorter et al. (2013) and Adusumilli et al. (2020) (Figure A2). As in observation-based (Dutrieux

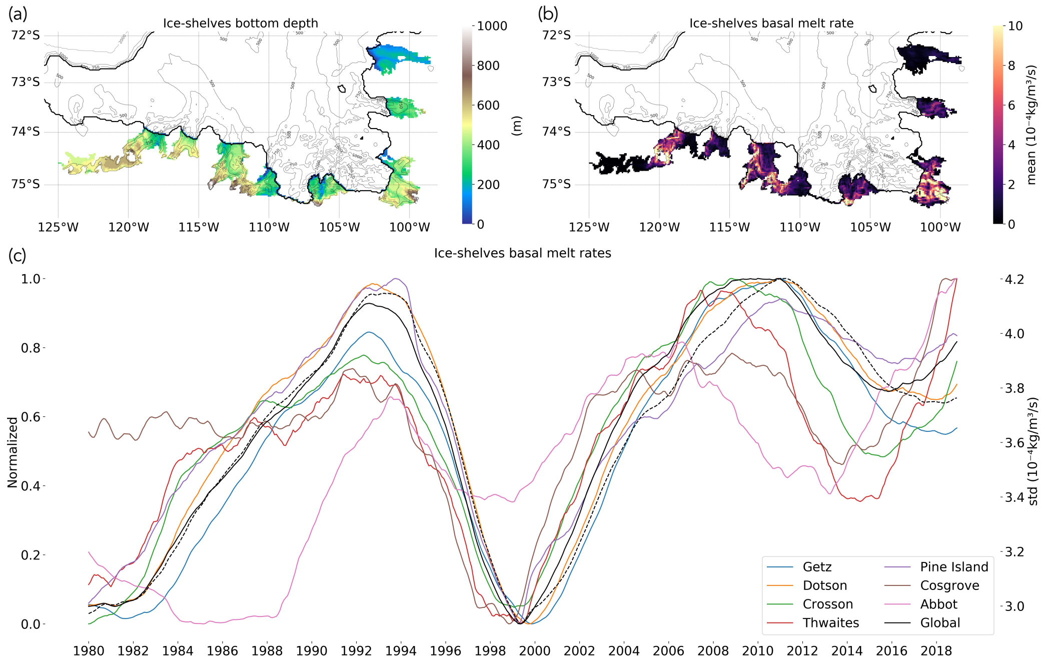

Figure 10. ice-shelf basal melt. (**a**) and (**b**) are maps of the Amundsen shelf showing the ice-shelves bottom depth (**a**) and the mean ice-shelf basal melt rate (**b**). For each of these maps, the bathymetry is represented at 500, 750, 1,100 and 2,000 m. The coastal margin and the shelf break line are displayed with a continuous line. (**c**) shows the ice-shelf basal melt rates variability between 1980 and 2018 with a 5-year running mean. The values for each ice-shelf are normalized between 0 and 1. The continuous black line shows the melt rate variability for all the considered ice-shelves and the dashed black line represents the associated standard deviation.

et al., 2014; Jenkins et al., 2018) and modelling (Kimura et al., 2017; Webber et al., 2019) studies, we find important interannual-to-decadal fluctuations of the basal melt rates. We notice that this variability is pretty similar for the different ice-shelves (Figure 10c). In particular, as observed by Dutrieux et al. (2014) and Jenkins et al. (2018) for Pine Island and Dotson, the ice-shelf basal melt rates decrease before 2000, reaching a minimum around 2000, before peaking in the late 2000s, followed by a decrease in the early 2010s. Note that the differences we observe for western Abbot are related to the very low basal depth of this ice-shelf (not shown). We also want to underline that, in this study, we are only interested in the low frequency variability, from interannual to decadal, since the ice flow of the glaciers outlet appears to be only slightly sensitive to high-frequency fluctuations (Christianson et al., 2016; Favier et al., 2019).

Given the similar evolution of melt rates across ice-shelves (Figure 10c), we consider the interannual-to-decadal variability of the total melt rate over all these ice-shelves in the following. A 40-year period is relatively short for an analysis of decadal variability, so the results in this section must be considered as a first analysis that will require further work. We report that the FWBI index leads the melt evolution by 21 months (Figure 11) with a relatively high lead-correlation (r=0.84). It is nonetheless not the best predictor of the low-frequency melt evolution. The aligned current just on the shelf, at the Do-Ge trough and near the seabed (at 411 m depth), corresponding to the so-called eastward "undercurrent", presents a low-frequency variability that explains most of the melt variance (r=0.97) 13 months ahead. The aligned current at 411 m at the eastern Pi-Th trough, just on the shelf, is also significantly correlated with the melt time series, with weaker correlations than for the eastward ”undercurrent” at the Do-Ge trough (r=0.89), but with a longer lead (37 months). This suggests that the current fluctuations at the shelf break occur at the eastern Pi-Th trough prior to the Do-Ge trough. The near-seafloor orthogonal current at the entry of the western Pi-Th trough (reached by a southern ACC branch) is also significantly anti-correlated (as southward velocities are negative) to the melt time series (and to the aligned-current characteristics, not shown) with a lag relatively close to the one found for the eastward ”undercurrent” at the eastern PI-Th trough (32 versus 37-month lead) - highlighting the possible important connection between the western and eastern Pi-Th troughs with an eastward ”undercurrent” detached from the shelf break in between these two Pi-Th troughs due to the bathymetry (Figures 3b,c and 12b). The surface aligned current off Do-Ge trough, representative of the ASC, is also significantly anti-correlated with the mean basal melt rate with a 32-month lead.

Note that we decided to show both the variability of the currents and the CT to try to independently understand their role at the shelf break instead of pouncing on thermal fluxes. Moreover, the data were not integrated over time to keep the focus on an in-depth characterization of the interannual-to-decadal fluctuations at the shelf break and not of the heat content on the continental shelf.

In summary, higher basal melt rates are preceded, on the one hand, by more CDW inflow in the western Pi-Th trough and an intensification of the ASC current just in front of the Do-Ge trough. On the other hand, an earlier intensification of the eastward ”undercurrent” at the eastern Pi-Th trough and then at the Do-Ge trough is apparent. Our results suggest a lag of 2 to 3 years between changes in the eastward ”undercurrent” or ASC and ice-shelf basal melt rates. Kimura et al. (2017) reported a few months for the connection from the shelf break to the ice-shelf base, with up to 7 months for Pine Island. We propose that longer lags at low frequency may be related to the accumulation and recirculation of warm water all over the continental shelf (CT on the shelf leads melt by only 5 months in Figure 11). Again, we acknowledge that our time window is relatively short to describe decadal variability, and there is probably a significant uncertainty on the estimated lags - in particular due to the use of 5-year running mean.

4 Discussion

We first further discuss possible mechanisms for the CDW inflow onto the Amundsen shelf, before paying attention to the more regional circulation. And finally, we question possible links between the interannual-to-decadal variability of the ice-shelf basal melt rates and climatic modes of variability.

4.1 CDW Intrusions onto the Shelf

The Amundsen Sea shelf break is located near the transition between the westerlies blowing over most of the Southern ocean and the easterlies blowing in the Antarctic coastal region. The corresponding Ekman transport creates a divergence of surface currents and a local sea surface height (SSH) minimum at the transition between the two wind regimes (Figure 12a). As reported in an earlier work (e.g., Thoma et al., 2008), this transition and associated divergence is strongest very close to the shelf break of the warm shelf zone, lifting up the CDW at the shelf break (Figure 12b). The divergence zone is further offshore in the case of the fresh shelf and therefore less suitable for CDW intrusions. As explained by Thompson et al. (2018), the dominant easterlies at the shelf break in this case induce an onshore SSH gradient, which favors the creation of the ASC in the east of Russell Bay.

We now extend this description by considering the effect of the sea-ice–ocean friction in the presence of consistent surface currents. As sea ice does not generally have the same velocity as surface currents, the relative speed difference between sea ice and sur-

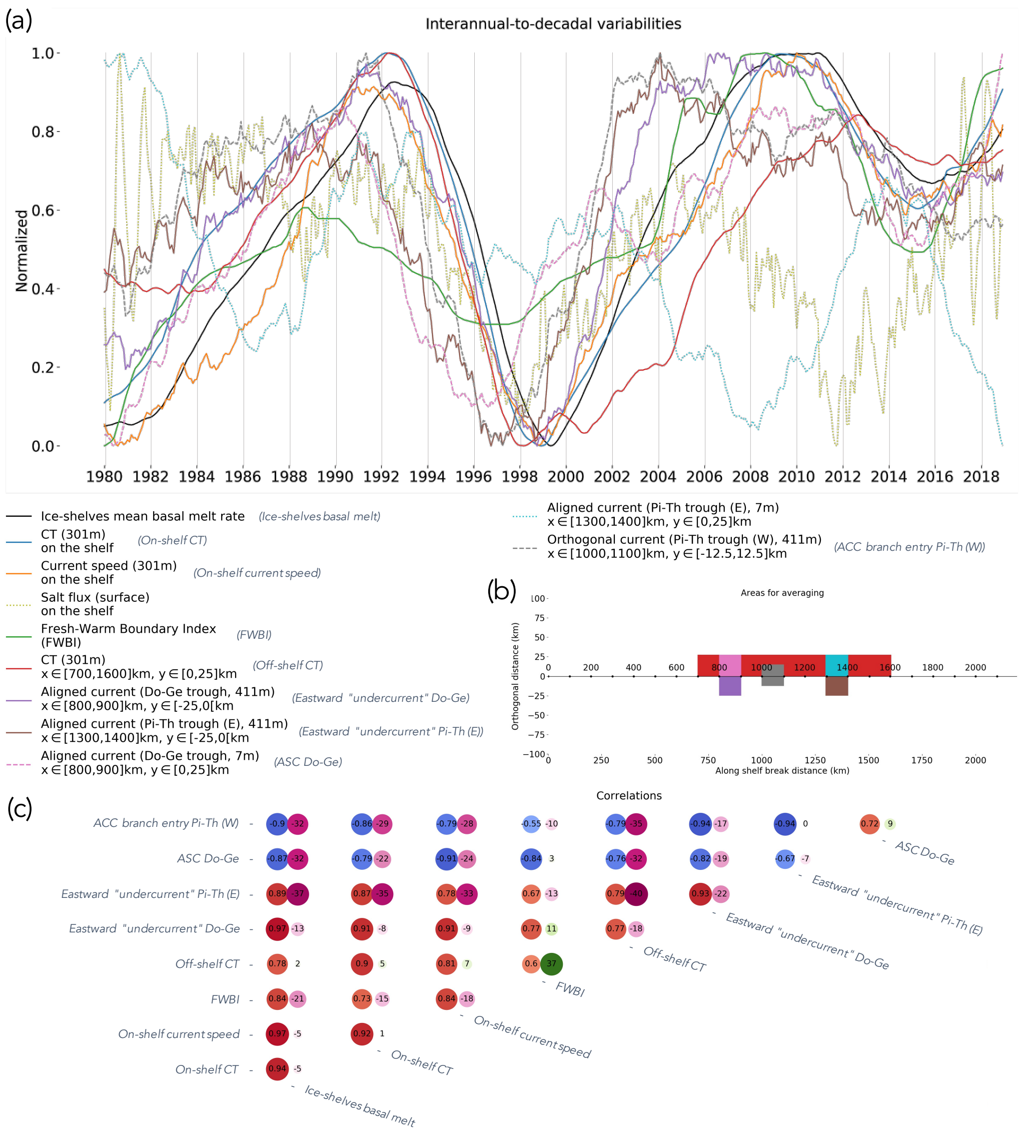

Figure 11. Correlations between the ocean state, either at the shelf break or on the shelf, and the ice-shelves mean basal melt rate. On the one hand, (**a**) shows the time series with a 5-year running mean of a chosen set of parameters averaged on areas colored (with the same color as for the time series) in the shelf break reference frame on (**b**), but for the values on the shelf - which are averaged on the blue zone colored in Figure 2. The dashed lines refer to parameters which are anti-correlated with the ice-shelves mean basal melt rate, and were then represented as $1 - [normalized\ values]$ to make the comparison more visual. On the other hand, (**c**) is a double entry table which indicates both the maximum correlation coefficient between the considered two time series and the lag (in months) associated to this correlation coefficient. The correlation coefficient is to the left with colors and sizes depending on its amplitude from blue to red. The lag is to the right with colors and sizes depending on its amplitude from pink to green. A negative (resp. positive) lag means that the considered parameter on the horizontal is in advance (resp. delayed) compared to the one on the vertical. The two dotted lines on (**a**) are not represented in this table due to their relatively weak correlation with the ice-shelves mean basal melt rate.

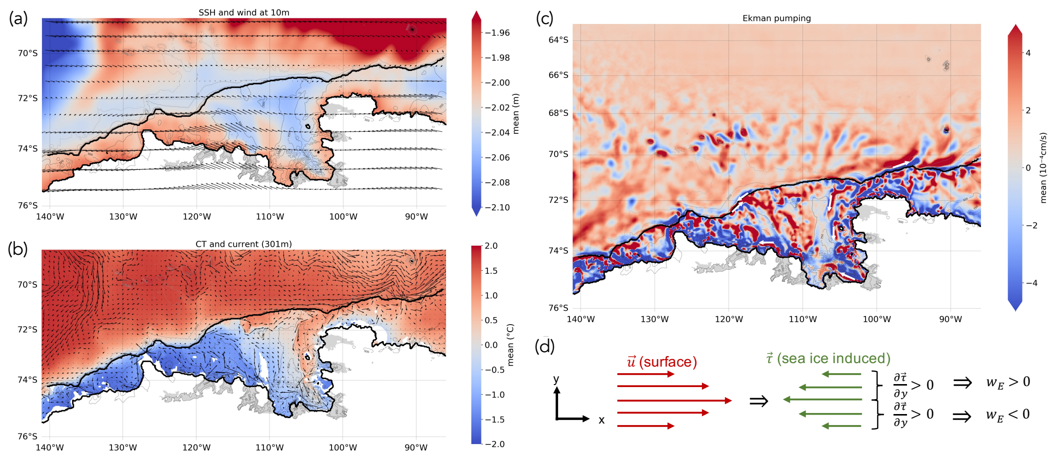

Figure 12. Effects of the top boundary of the ocean. (**a**) mean SSH (slightly saturated to focus on the continental shelf and the shelf break) with the mean wind over the region. (**b**) mean CT at 301 m depth (shaded) and mean currents at the same depth (black arrows). The ice-shelves of interest in this study are shaded in grey whereas the others are not represented. (**c**) mean Ekman pumping calculated from the ocean surface stress - induced either by the wind or the sea ice. Some white arrows are drawn in order to show the consistent surface currents at a few locations. The coastal margin and the shelf break are represented with a continuous black line. (**d**) Schematics of the effect of sea ice on ekman pumping.

face currents favors an upwelling on the left side of surface currents, and a downwelling on the right side (Gupta et al. (2020) showed the same effect for vortices). Several examples of the occurrence of such process are indicated in Figure 12c, and schematized in Figure 12d. Because of the strong currents at the shelf break, this process might play a significant role in cross-shelf energy exchange. In particluar, this favors an upwelling at the entrance of the Do-Ge trough.

Bottom Ekman pumping was also suggested to play a role on the onshore advection of CDW. Wåhlin et al. (2012) inferred from observations in the western Amundsen region that the baroclinic structure of the ACC branch along the shelf break would lead to a near-bottom onshelf Ekman transport. Even though we report that the bottom friction is probably partly misrepresented due to the low vertical resolution near the seafloor in our simulation, we point out that this effect could play a key role at the entry of the Do-Ge trough where the eastward "undercurrent" is licking the continental slope (Figure 4c). In particular, we observe at this location an uplift of the isopycnals, which indicates an upward transport of water from greater depth along the slope (Figure 4a).

Finally, branches of the ACC may contribute to bring CDW onto the continental shelf, with pathways highly influenced by the bathymetry. A northern branch directly reaches the vicinity of the shelf break in the western part of the Bellingshausen Sea (Figure 12b), as previously described by Orsi et al. (1995). For the Amundsen Sea, we point out a southern ACC branch that follows the eastern flank of the Ross Gyre (negative SSH anomaly near the western domain boundary in Figure 12a) and flows eastward along the shelf break, north of the ASC. This branch then splits into a pathway closer to the shelf break, with a great meander in the east of Russell Bay just before reaching the shelf break to the west of the western Pi-Th trough (Figure 12a,b; see also Appendix Appendix B), and another pathway further north that impacts the shelf break between the western and eastern Pi-Th troughs (Figure 12a,b). Figure 3d,e shows that the thermocline top and bottom are relatively uniform along the southern ACC branch, with a shallow thermocline favoring CDW intrusions onto the warm shelf. The role of the Ross Gyre in the CDW penetrations was also suggested by Nakayama et al. (2018) and Armitage et al. (2018). Although the interaction of this southern ACC branch with the western PI-Th topography seems constant over time (B1), intermittent events during which this ACC branch is stuck at the shelf break at the entry of the Do-Ge trough (see Section 3.2) could also favor CDW intrusions in the fresh shelf region.

In summary, our analysis of the mean ocean state at the shelf break has led to the suggestion of four different mechanisms for the CDW intrusion onto the Amundsen shelf, from the Ekman pumping induced by the wind to the one induced by the sea ice effect passing by the effect of topography at the entry of a trough and the Ekman bottom friction along the continental shelf. These mechanisms at fresh and warm shelves are also schematized in Figure 6. Note that the high frequency processes, which could also play a significant role in the CDW inflow - such as the development of baroclinic instabilities along the shelf break - were left aside in this analysis.

4.2 Regional Circulation

We propose a schematic of the main circulation and pathways in Figure 13. Although oversimplistic, it can be used to discuss the reasons for high melt rates in the mean fresh shelf area. We identify two distinct cyclonic recirculations on the Amundsen shelf, one in the fresh shelf zone, essentially feeding Dotson and Getz in terms of available heat for melt, and one in the warm shelf zone, essentially feeding Abbot, Cosgrove, Pine Island, Thwaites and Crosson. Jourdain et al. (2017) found that only 6 to 31 % of the heat that enters the Amundsen cavities with melting potential is actually used to melt the ice-shelves, so the Antarctic Coastal Current may transport the remaining heat to the following cavities. We therefore suggest that such connectivity may, at least partly, explain that Getz and Dotson behave like warm cavities in spite of being in the fresh shelf area. This is supported by the modelling study by Kimura et al. (2017) who did not identify heat anomaly propagation along the Do-Ge trough leading to Dotson ice-shelf (their Figure 7). We also suggest that a part of the return current of the cyclonic circulation in the main troughs (Do-Ge and Pi-Th) are reoriented towards the eastward "undercurrent" forming recirculation cells, which may contribute to a relatively slow build up of warm temperatures over the entire continental shelf (Figure 13).

The connectivity with the Ross and Bellingshausen Seas may also be key in the understanding of the ocean dynamics in the region, with a part of the meltwater from the Bellingshausen Sea advected into the Amundsen Sea, and a large part of the meltwater from the Amundsen Sea advected into the Ross Sea (Nakayama et al., 2014). On the one hand, the connection from the Bellingshausen Sea occurs through the Antarctic Coastal Current flowing along Abbot ice-shelf, and intermittently through the ASC at the shelf break - when it is initiated further to the Bellingshausen Sea. On the other hand, the connection to the Ross Sea seems quite different, as a part of the Antarctic Coastal Current mixes with the ASC, and even intensifies this westward current - likely because of the tight continental shelf around Siple Island - making the ASC constant through time at this location and further to the west.

We also stress the important role of the variability west of Russell Bay. It is not simply the transition zone between the mean fresh and warm shelves, but it also corresponds to the junction zone between the two on-shelf recirculations and where the ACC branch initiated to the south-east of the Ross Gyre impacts the shelf (Figure 13). We reckon that most of the ocean variability on the Amundsen shelf, and thus most of the low frequency variability of the basal melt activity underneath the ice-shelves of the region, could be driven by processes impacting this complex region. Three different vari-

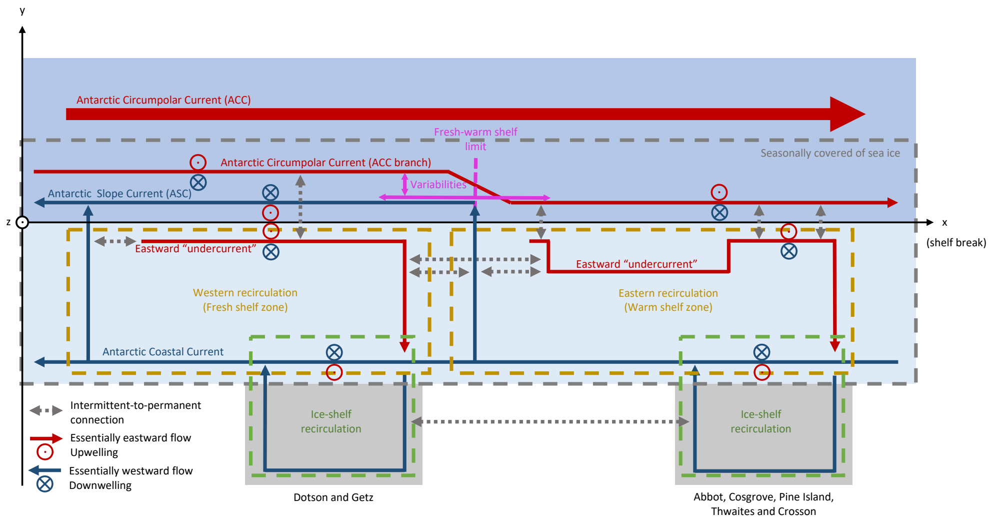

Figure 13. Schematic of the circulation in the Amundsen Sea pointing out the fresh and warm shelves and their connectivity.

ables in the Russell Bay area seem to be key and partly interacting: the CT at the shelf break, the intensity of the outflow from the shelf - likely initiating the ASC -, and the impact location of the ACC branch. A complex mixture of processes occur there, as, e.g., the sea ice induced Ekman pumping associated to the ASC, favoring a shallowing of the thermocline at the shelf break and thus a positive CT anomaly at the entry of the Do-Ge trough. A strong ASC may also prevent the ACC branch from impacting the shelf break further to the west of Russel Bay, while a strong ACC branch may block the outflow from the shelf. The FWBI index developed in our analysis enables an overall description of the resulting variability in the fresh-warm shelf boundary, using surface ocean data to infer currents anomalies in the area. In a nutshell, this index could likely meet, at least partly, a need of remote control of shelf properties and ice-shelf basal melt rates in the region (Thompson et al., 2020).

4.3 Link with Climatic Modes of Variability

The aforementioned recirculations over the continental shelf may explain the multi-year lag between low-frequency current anomalies at the shelf break and low-frequency ice-shelf basal melt, as onshore CDW transport anomalies would need several years to build up a large warm water volume over the continental shelf. This would possibly act as a filter on the effects of higher-frequency wind stress anomalies at the shelf break, in particular those associated with El Niño-Southern Oscillation (ENSO, Holland et al., 2019) and the Southern Annular Mode (SAM). Using the multivariate ENSO Index (MEI.v2) - provided by the NOAA (`https://psl.noaa.gov/enso/mei/`) - and the SAM index - provided by the British Antarctic Survey (`https://legacy.bas.ac.uk/met/gjma/sam.html`) - with a 5-year running mean and detrended (Figure 14), we report that, over the duration of our simulation, the anti-correlation coefficient with the ice-shelves mean basal melt rate is lower in absolute value for MEI than SAM (-0.52 and -0.68 respectively). However, for the period starting in 2005, this anti-correlation climbs to -0.94 for MEI whereas it stays almost the same for SAM (-0.72). Therefore, the period starting in 2005 could be partly misleading regarding the possible direct effect of ENSO on the basal melt activity in the Amundsen region. Following Armitage et al. (2018), we point out the possible effect of the combination of ENSO and SAM on the basal melt activity in the re-

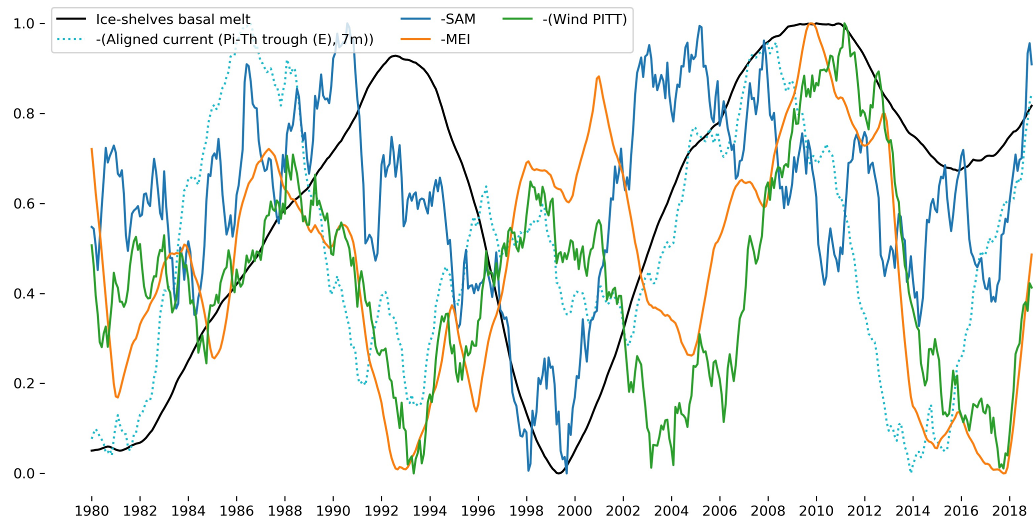

Figure 14. Connection with the different modes of climate variability. The PITT box is defined as in Holland et al. (2019), extending over 115°-102°W, 71.8°-70.2°S

gion, in particular to explain the drop in the ice-shelf basal melt rate around 2000. However, we stress the decorrelation between the variability of the aligned current off eastern Pi-Th trough and the basal melt activity (Figure 11a). In fact, this ACC branch along the shelf break presents a relatively good correlation with MEI (0.80, Figure 14), and especially a similar trend towards a weakening of this current. Therefore, not only the fluctuations of the wind in the PITT box - defined by Holland et al. (2019) - follow the ENSO variations, but the ACC branch along the shelf break at the entry of the eastern Pi-Th trough also seems to be in phase with this variability. However, in contrast to the assumption of Holland et al. (2019), ice-shelves melt rates are not in phase with these variations. A possible explanation is that the negative meridional density gradient at depth at the shelf break in this zone might impeach possible interactions with the offshore ACC branch.

Finally, we have found that the FWBI has an eastward trend (Figure 9), which might be linked to wind changes in Russel Bay area as well as to increasing outflow of water between the Do-Ge trough and the western Pi-Th one. This is coherent with a strengthening of the ASC, and thus in agreement with the observed negative MEI trend as opposed to the positive SAM trend - which would entail a strengthening of the ACC (Armitage et al., 2018). It is unclear whether such drift could continue and extend beyond the location where the ACC branch generally impacts the shelf break. The role of the different modes of climate variability could be of high importance in this specific area in the east of Russell Bay. And we think that the use of our suggested FWBI could be useful for future work on these topics.

A global overview of the winds and the ocean dynamics in the Amundsen Sea is shown in Figure 15.

5 Conclusion

In this paper, we have used a regional ocean simulation to revisit the ocean circulation in the Amundsen Sea with a focus on the continental shelf break, and an attempt to link the ocean variability along this bathymetric feature with the ice-shelf basal melt-

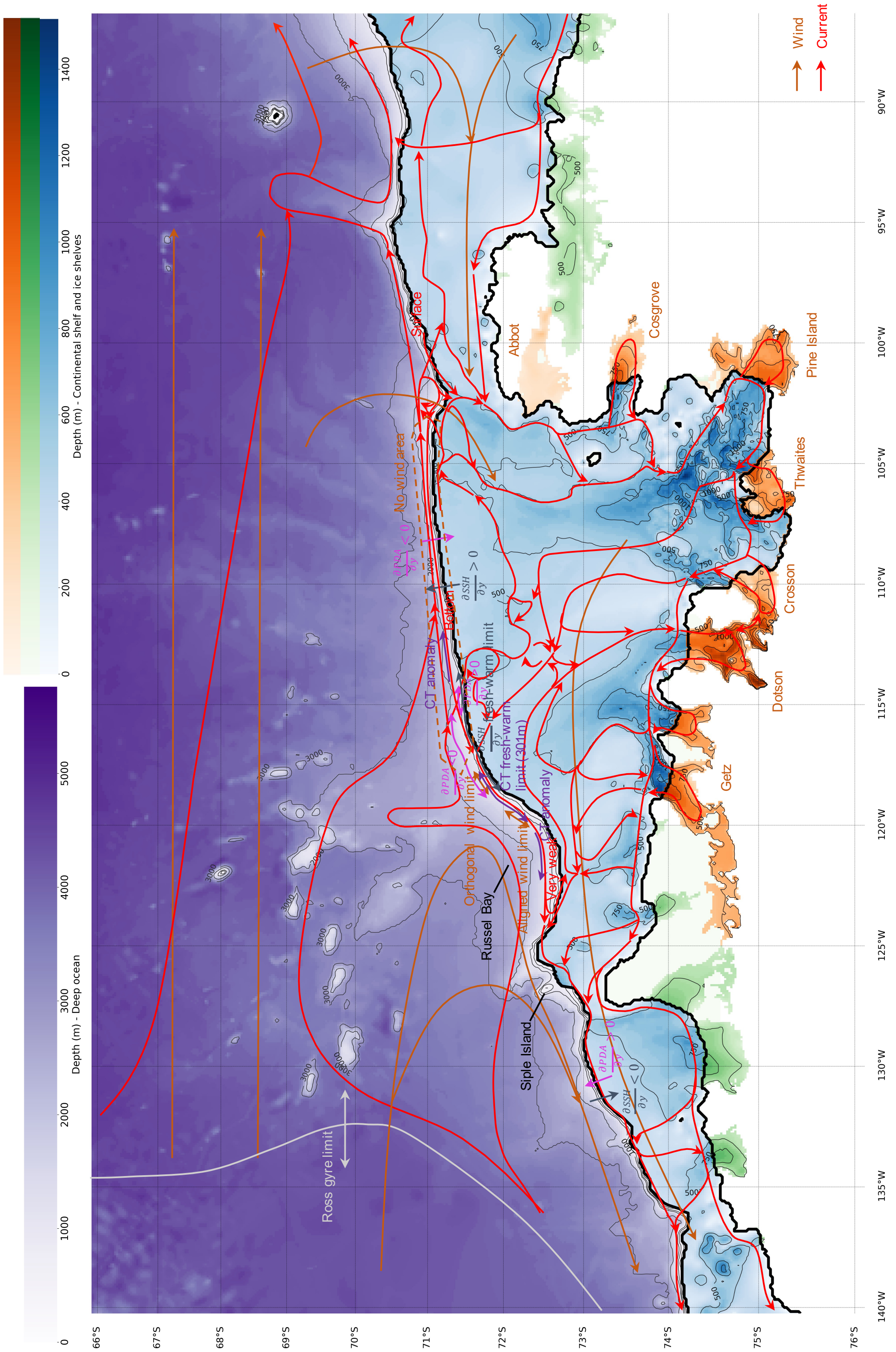

Figure 15. Global overview of the winds and the ocean dynamics in the Amundsen Sea. The deep ocean, the shelf and both the ice-shelves of interest for this study and the others are are in purple, blue, orange and green color scales, respectively. The coastal margin and the shelf break are represented with continuous black lines.

ing. In particular, we have developed a methodology to study the ocean state in the reference frame of the continental shelf break.

In the mean state, the western Amundsen Sea (westward of Russel Bay) is characterized as a fresh shelf, with a limited presence of CDW onshore, an eastward "undercurrent" at the edge of the shelf and the ASC in off-shelf surface waters. On the other hand, the eastern Amundsen Sea is characterized as a warm shelf with an important volume of CDW onshore, an eastward current at the edge of the shelf, and eastward ACC branches reaching the shelf break. Despite being located in the mean fresh shelf area, the Getz and Dotson ice-shelves experience melt rates of comparable magnitude as Thwaites and Pine Island in the warm shelf area, and they all undergo a similar decadal variability.

To analyze the interannual-to-decadal variability, we have created the Fresh-Warm Boundary Index (FWBI) that delineates the fresh-warm shelf limit through time, in a way that could potentially be estimated from satellite data. FWBI oscillates between 800 and 1100 km over 1980-2018, with a trend corresponding to an eastward drift towards the entry of the Pi-Th western trough. At decadal time scales, FWBI leads the ice-shelf basal melt evolution by 21 months with a relatively high lead-correlation (r=0.84). However, it is difficult to assess whether this is a fortuitous correlation (e.g., due to large scale atmospheric forcing with a coherent structure over the Amundsen Sea) or a relevant relationship.

In addition to processes that have already been pointed out to be important for onshore CDW intrusions (Ekman transport induced by wind or bottom friction), we propose that Ekman pumping associated with consistent currents under sea ice may be important at the shelf break, especially at the entry of the Do-Ge trough. We also suggest a control of onshore CDW intrusions by a southern ACC branch - initiated to the southeast of the Ross Gyre - that reaches the shelf break in the Amundsen region, with a strong role of topography. After a careful examination of the current systems and connections, we suggest that most of the inflow onto the continental shelf happens at the entry of the western Pi-Th trough, where the topography enables the southern ACC branch to impact the shelf break to the east of Russel Bay. The Antarctic Coastal Current would then carry part of the heat available for melt towards the fresh shelf zone, with possible recirculations both in the Do-Ge trough and in the Pi-Th trough, which are suggested to explain a multi-year lag between low-frequency anomalies at the shelf break and ice-shelf basal melt, although longer simulations may be needed to confirm this result.

Finally, based on our simulations, we have proposed a schematic of the vertical structure of currents near the fresh versus warm shelves (Figure 6), of the main CDW pathways (Figure 15), and of the main connections over the continental shelf (Figure 13), which may be a useful base for future work.

Appendix A Evaluation of the Simulation

In order to evaluate our simulation, we compare it with satellite products and *in situ* observations.

A1 Sea Ice Cover

First, we use the sea ice concentrations from remote sensing data (Peng et al. (2013) updated, NOAA/NSIDC Climate Data Record). We calculate the sea ice extent (SIE) only considering sea ice concentration (SIC) values greater than 0.15 (as the uncertainty for lower values is relatively high) and at locations that are defined as ocean points in both the remote sensing and model data.

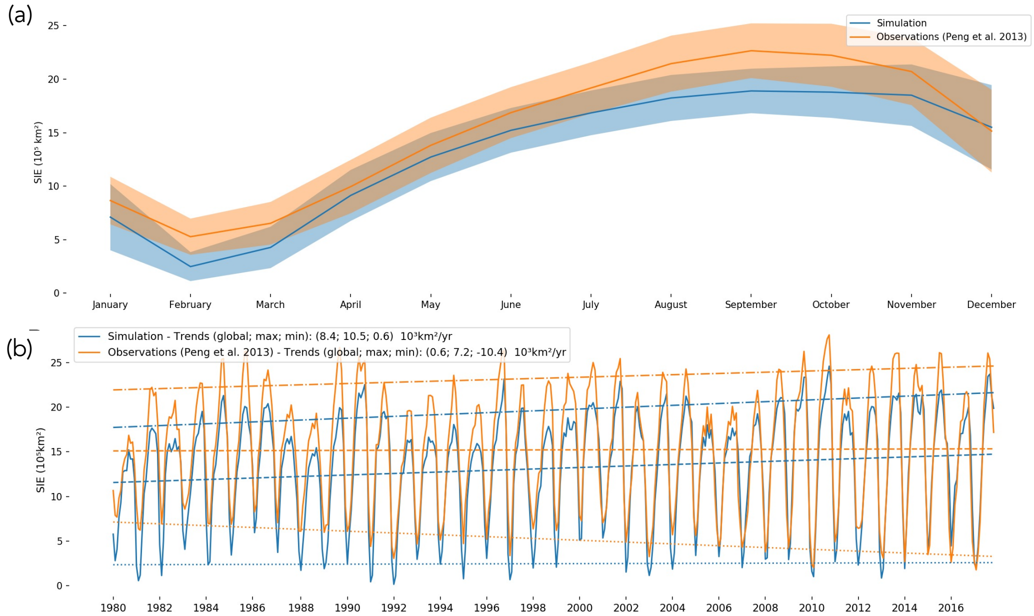

Figure A1. Sea ice evaluation: focus on the SIE. Note that we consider that there is actually sea ice on the top of the ocean when the SIC is superior to 0.15. We show the evaluation of the SIE for our simulation and the satellite observations (Peng et al. (2013) updated) through the representation of the SIE climatology (**a**). The SIE time series of our simulation and the observations are displayed on (**b**) with the global, maximum and minimum trends.

The average seasonal SIE is relatively well represented by our simulation, despite an underestimation by about 16 % over the studied period (Figure A1a). The trend and interannual variability of the maxium annual SIE is also well reproduced (Figure A1b). This is however not the case of the annual SIE minimum that has a negative trend in our simulation but not in the remote sensing product.

A2 ice-shelf basal melt Rates

Then, we focus on the ice-shelf basal melt rates and compare them with the dataset produced by Rignot et al. (2013) and Depoorter et al. (2013) based on remote sensing data and firn simulations (Figure A2). Our simulated melt rates are slightly higher than the remote sensing estimates by about 0.37×10^{-4} $kg/m^2/s$ for Getz to about 1.11×10^{-4} $kg/m^2/s$ for Abbot for the period 2003-2008 (Thwaites left apart). We strongly underestimate melt rates underneath Thwaites, which may be related to the fact that our ice-shelf topography is from BedMachine-Antarctica (Morlighem et al., 2020) and is representative of the recent years, while Rignot et al. (2013) and Depoorter et al. (2013) used an older topography. Large ice thinning and front retreat has indeed occurred at Thwaites in the mid 2010s (Alley et al., 2021), which may reduce local melt rates (Donat-Magnin et al., 2017).

A3 Temperature and Salinity

Finally, we compare our simulation to the conservative temperature (CT) and absolute salinity (AS) profiles collected on the Amundsen Sea continental shelf over 1994-2018 (Dutrieux et al., 2014; Jenkins et al., 2018). The location of individual profiles is shown in Figure A3a. Simulated CT is overestimated by no more than 0.5 °C (Figure A3b,c),

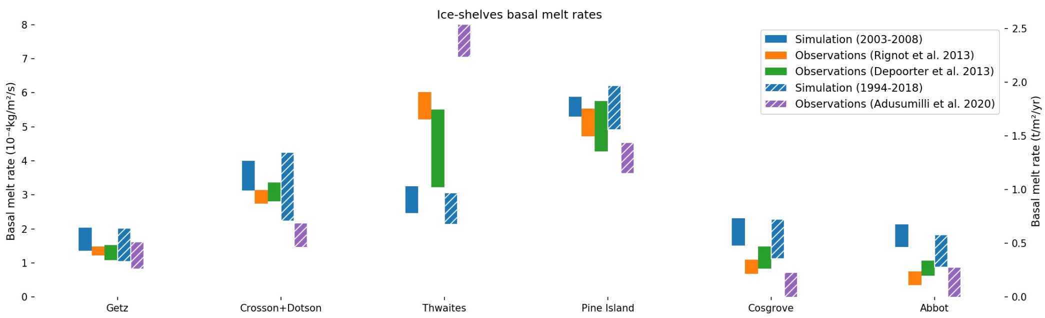

Figure A2. Evaluation of the ice-shelf basal melt rates for our simulation and the observational estimates from (Rignot et al., 2013) and (Depoorter et al., 2013) for the period 2003-2008, and from (Adusumilli et al., 2020) for the period 1994-2018. The middle of the bars indicate the mean values over the considered period, while their height indicates the associated standard deviation (mean value ± std value).

and winter water (WW) tends to be slightly too salty in our simulations while CDW tends to be slightly too fresh (Figure A3b,d). The CT overestimation above the thermocline is in accordance with the global underestimation of sea ice. This overestimation results in a slightly thinner and shallower thermocline (as defined in the caption of Figure 3) for the simulations compared to the observations.

Overall, we conclude that our simulation is suitable to conduct the analysis we present in this paper, and that our results can be interpreted in a realistic context.

Appendix B Cross-sections

We share additional cross-sections climatologies of the along-shelf ocean velocity in between the Do-Ge trough and the western PI-Th trough (Figure B1) in order to put our simulation in perspective with observations from ? (?)their Figure 6]walker2013oceanographic, and to stress the role of the southern ACC branch initiated to the south-east of the Ross Gyre. Indeed, this branch can be spotted on the cross-section at x=910 km for y∈[20, 55] km around 300 m, and it impacts the shelf break around x=1030 km, initiating a strong eastward undercurrent at the entry of the western PI-Th trough. In addition, we show the same cross-sections for the CT (Figure B2) to underline the deepening of the thermocline from east to west and the consistency of the vertical cold to warm waters limit at ˜27.55 kg/m^3. Finally, we display the along-shelf thermal flux (Figure B3) expressed by $\Phi_{x,th} = \rho_w c_{pw} \Gamma_T \sqrt{C_D} u(CT - CT_{ref})$ where $\rho_w = 1026\ kg.m^{-3}$, $c_{pw} = 3992\ J.kg^{-1}.K^{-1}$ (see also Tab. 1 and Jourdain et al. (2017)) and with a reference CT set to -2 °C. It enables to keep the sign of the thermal flux associated to the aligned current and to focus on the thermal flux below the thermocline, in the CDW zone.

Appendix C Movies

C1 Supplementary: "Aligned_current_Oxz_Oxy.mp4"

Movie showing, through time, the aligned current in an (Oxz) reference frame for the top panel and an (Oxy) reference frame for the bottom panel. On the one hand, the top panel focuses on the aligned current just off the continental shelf, averaged along the orthogonal direction (0<y<25 km). And on the other hand, the bottom panel gives a broader overview of the aligned current at 301 m close to the shelf break (marked with

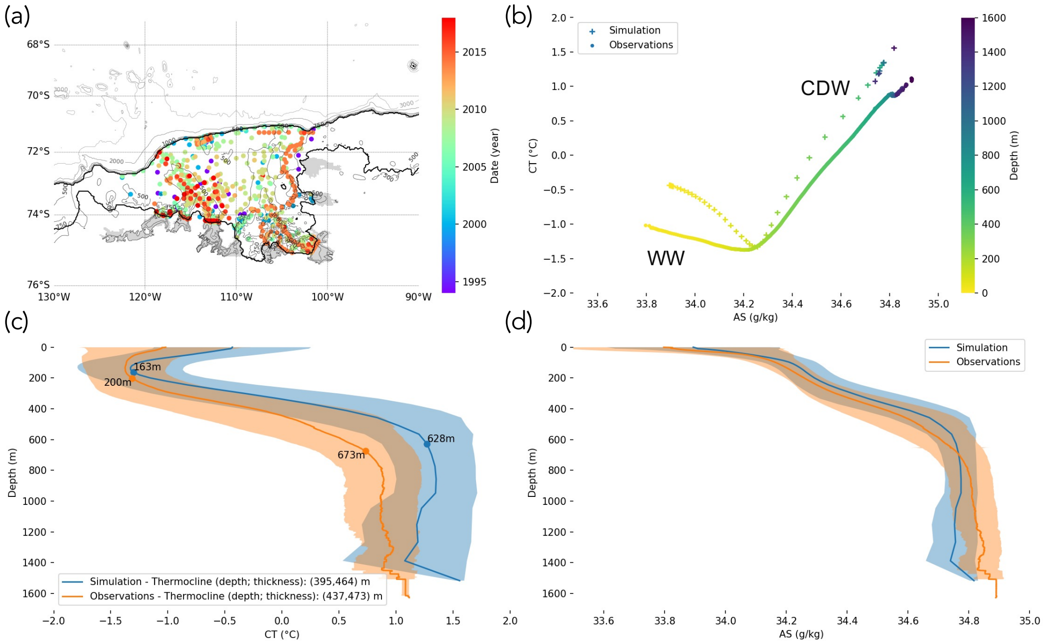

Figure A3. Evaluation of the ocean temperature and salinity. We show on (**a**) the map of the CTD data collected (Dutrieux et al. (2014) updated) on the continental shelf - delineated as in Figure 2a - between 1994 and 2018 (cf. colors). The mean T-S diagram, with the CT and AS, for all those CTD locations is displayed on (**b**) for both our simulation and the observations, with colors referring to the depth. Finally, we display the associated mean CT profiles (**c**) (resp. AS profiles (**d**)) for our simulation and the observations with the thermocline characteristics annotated on the CT profiles.

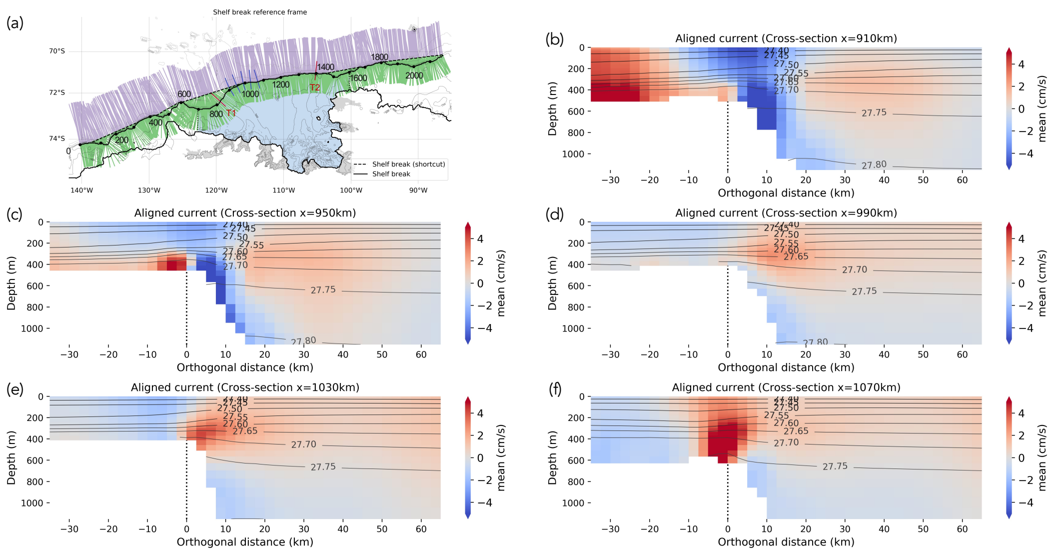

Figure B1. From Do-Ge trough to western PI-Th trough. We show on (**a**) the shelf break reference frame as on Figure 2a, with the blue lines corresponding to the five cross-sections considered on (**b-f**, from west to east) showing the climatologies of the along-shelf velocity. In panels (**b-f**), a red (resp. blue) color means that the current is globally eastward (resp. westward). Isopycnals (potential density anomalies) are plotted every 0.05 kg.m-3 and the identified shelf break is shown as a dotted black line at y=0 km.

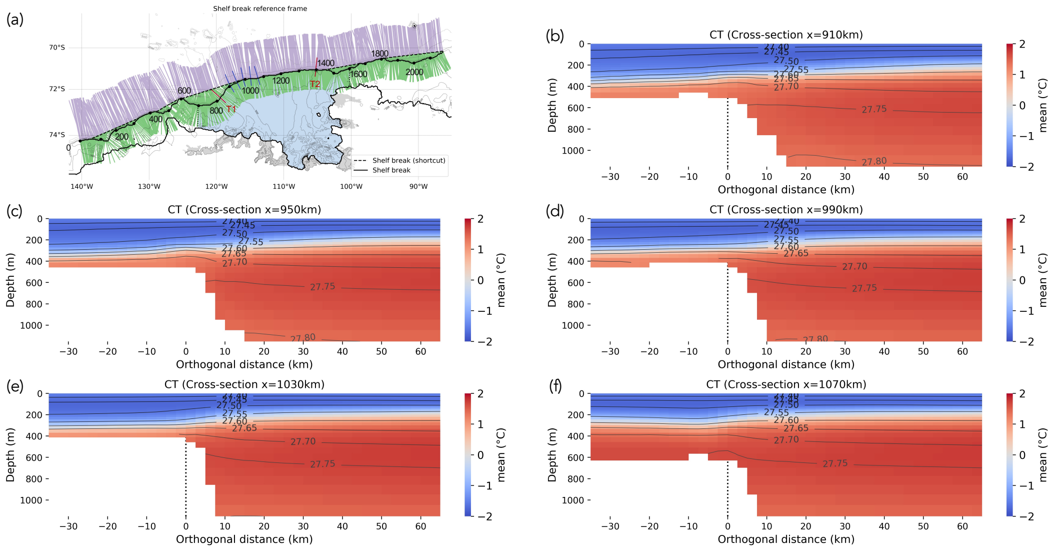

Figure B2. From Do-Ge trough to western PI-Th trough. Same as B1 but for the CT.

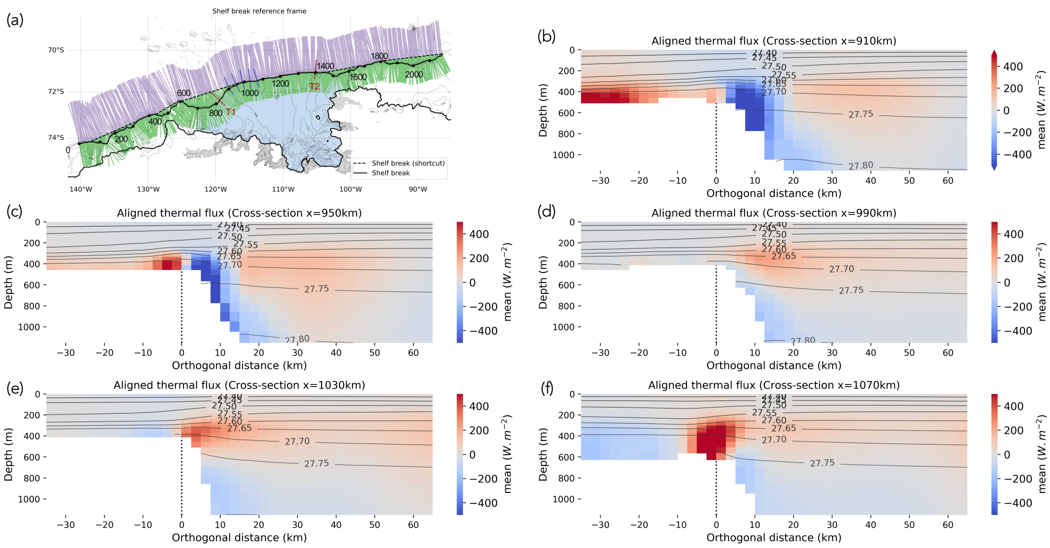

Figure B3. From Do-Ge trough to western PI-Th trough. Same as B1 but for the aligned thermal flux. A red (resp. blue) color means that the thermal flux is globally eastward (resp. westward).

a continuous black line at y=0 km with markers every 100 km). On both panels, the western and very eastern extremities of Russel Bay are marked, either by vertical lines (top) or by squares (bottom). Finally, the two cross-sections in this study are drawn on the bottom panel.

C2 Supplementary: "Aligned_current_T1_T2.mp4"

Movie displaying the aligned current at the shelf break of the two cross-sections (T1: top left panel, T2: bottom left panel) from January 1980 to December 2018 (mean state represented on Figure 4). In addition, a third panel was built to give insights on the vertical structure of the eastward "undercurrent" at the extremity of the continental shelf (see Section 3.1). For every month, the aligned current was averaged along the orthogonal direction ($-15<y<0$ km) for the two cross-sections, and both a barotropic component (markers at the top) and a baroclinic component (curves) were extracted.

Acknowledgments

This research was supported by the European Union's Horizon 2020 research and innovation programme under grant agreement number 820575 (TiPACCs) and by the ANR-19-CE01-0015 project (EIS). This work was granted access to the HPC resources of CINES under the allocations DARI n°A0100106035 and n°A0080106035 made by GENCI.

Data Availability Statement: All the elements required to reproduce our simulation are available on `https://doi.org/10.5281/zenodo.5521569`.

Author contributions (CRediT): **Alban Planchat**: Conceptualization, Investigation, Methodology, Formal analysis, Visualization and Writing – original draft – **Nicolas C. Jourdain**: Supervision, Funding acquisition, Methodology, Resources, Conceptualization and Writing – original draft – **Pierre Dutrieux**: Methodology and Writing – review & editing –

References

Adusumilli, S., Fricker, H. A., Medley, B., Padman, L., & Siegfried, M. R. (2020). Interannual variations in meltwater input to the southern ocean from antarctic ice shelves. *Nature geoscience*, *13*(9), 616–620.

Alley, K. E., Wild, C. T., Luckman, A., Scambos, T. A., Truffer, M., Pettit, E. C., ... others (2021). Two decades of dynamic change and progressive destabilization on the thwaites eastern ice shelf. *The Cryosphere Discussions*, 1–31.

Armitage, T. W., Kwok, R., Thompson, A. F., & Cunningham, G. (2018). Dynamic topography and sea level anomalies of the southern ocean: Variability and teleconnections. *Journal of Geophysical Research: Oceans*, *123*(1), 613–630.

Assmann, K., Jenkins, A., Shoosmith, D., Walker, D., Jacobs, S., & Nicholls, K. (2013). Variability of circumpolar deep water transport onto the amundsen sea continental shelf through a shelf break trough. *Journal of Geophysical Research: Oceans*, *118*(12), 6603–6620.

Carrère, L., Lyard, F., Cancet, M., Guillot, A., & Roblou, L. (2012). Fes2012: A new global tidal model taking advantage of nearly twenty years of altimetry. In *Proceedings of the 20 years of progress in radar altimetry symposium (venice, italy)* (pp. 1–20).

Christianson, K., Bushuk, M., Dutrieux, P., Parizek, B. R., Joughin, I. R., Alley, R. B., ... others (2016). Sensitivity of pine island glacier to observed ocean forcing. *Geophysical Research Letters*, *43*(20), 10–817.

Dee, D. P., Uppala, S. M., Simmons, A., Berrisford, P., Poli, P., Kobayashi, S., ... others (2011). The era-interim reanalysis: Configuration and performance of the data assimilation system. *Quarterly Journal of the royal meteorological society*, *137*(656), 553–597.

Depoorter, M. A., Bamber, J., Griggs, J., Lenaerts, J. T., Ligtenberg, S. R., van den Broeke, M. R., & Moholdt, G. (2013). Calving fluxes and basal melt rates of antarctic ice shelves. *Nature*, *502*(7469), 89–92.

Donat-Magnin, M., Jourdain, N. C., Spence, P., Le Sommer, J., Gallée, H., & Durand, G. (2017). Ice-shelf melt response to changing winds and glacier dynamics in the amundsen sea sector, antarctica. *Journal of Geophysical Research: Oceans*, *122*(12), 10206–10224.

Dotto, T. S., Garabato, A. C. N., Bacon, S., Holland, P. R., Kimura, S., Firing, Y. L., ... Jenkins, A. (2019). Wind-driven processes controlling oceanic heat delivery to the amundsen sea, antarctica. *Journal of Physical Oceanography*, *49*(11), 2829–2849.

Dotto, T. S., Naveira Garabato, A. C., Wåhlin, A. K., Bacon, S., Holland, P. R., Kimura, S., ... Jenkins, A. (2020). Control of the oceanic heat content of the getz-dotson trough, antarctica, by the amundsen sea low. *Journal of Geophysical Research: Oceans*, *125*(8), e2020JC016113.

Dussin, R., Barnier, B., Brodeau, L., & Molines, J. (2016). The making of the drakkar forcing set dfs5. *DRAKKAR/MyOcean Rep*, 01–04.

Dutrieux, P., De Rydt, J., Jenkins, A., Holland, P. R., Ha, H. K., Lee, S. H., ... Schröder, M. (2014). Strong sensitivity of pine island ice-shelf melting to climatic variability. *Science*, *343*(6167), 174–178.

Favier, L., Jourdain, N. C., Jenkins, A., Merino, N., Durand, G., Gagliardini, O., ... Mathiot, P. (2019). Assessment of sub-shelf melting parameterisations using the ocean–ice-sheet coupled model nemo (v3. 6)–elmer/ice (v8. 3). *Geoscientific Model Development*, *12*(6), 2255–2283.

Gupta, M., Marshall, J., Song, H., Campin, J.-M., & Meneghello, G. (2020). Sea-ice melt driven by ice-ocean stresses on the mesoscale. *Journal of Geophysical Research: Oceans*, *125*(11), e2020JC016404.

Holland, P. R., Bracegirdle, T. J., Dutrieux, P., Jenkins, A., & Steig, E. J. (2019). West antarctic ice loss influenced by internal climate variability and anthropogenic forcing. *Nature Geoscience*, *12*(9), 718–724.

Jacobs, S., Giulivi, C., Dutrieux, P., Rignot, E., Nitsche, F., & Mouginot, J. (2013). Getz ice shelf melting response to changes in ocean forcing. *Journal of Geophysical Research: Oceans*, *118*(9), 4152–4168.

Jenkins, A., Shoosmith, D., Dutrieux, P., Jacobs, S., Kim, T. W., Lee, S. H., ... Stammerjohn, S. (2018). West antarctic ice sheet retreat in the amundsen sea driven by decadal oceanic variability. *Nature Geoscience*, *11*(10), 733–738.

Jourdain, N. C., Mathiot, P., Merino, N., Durand, G., Le Sommer, J., Spence, P., ... Madec, G. (2017). Ocean circulation and sea-ice thinning induced by melting ice shelves in the amundsen sea. *Journal of Geophysical Research: Oceans*, *122*(3), 2550–2573.

Jourdain, N. C., Molines, J.-M., Le Sommer, J., Mathiot, P., Chanut, J., de Lavergne, C., & Madec, G. (2019). Simulating or prescribing the influence of tides on the amundsen sea ice shelves. *Ocean Modelling*, *133*, 44–55.

Kim, T.-W., Ha, H. K., Wåhlin, A., Lee, S., Kim, C.-S., Lee, J. H., & Cho, Y.-K. (2017). Is ekman pumping responsible for the seasonal variation of warm circumpolar deep water in the amundsen sea? *Continental Shelf Research*, *132*, 38–48.

Kimura, S., Jenkins, A., Regan, H., Holland, P. R., Assmann, K. M., Whitt, D. B., ... Dutrieux, P. (2017). Oceanographic controls on the variability of ice-shelf basal melting and circulation of glacial meltwater in the amundsen sea embayment, antarctica. *Journal of Geophysical Research: Oceans*, *122*(12), 10131–10155.

Lyard, F., Lefevre, F., Letellier, T., & Francis, O. (2006). Modelling the global ocean tides: modern insights from fes2004. *Ocean dynamics*, *56*(5-6), 394–415.

Madec, G. (2016). the nemo team: Nemo ocean engine. *Note du Pôle de modélisation, Institut Pierre-Simon Laplace (IPSL), France*, *27*, 1288–1619.

Marsh, R., Ivchenko, V., Skliris, N., Alderson, S., Bigg, G. R., Madec, G., … others (2015). Nemo–icb (v1. 0): interactive icebergs in the nemo ocean model globally configured at eddy-permitting resolution. *Geoscientific Model Development*, *8*(5), 1547–1562.

Mathiot, P., Jenkins, A., Harris, C., & Madec, G. (2017). Explicit representation and parametrised impacts of under ice shelf seas in the z coordinate ocean model nemo 3.6. *Geoscientific Model Development*, *10*(7), 2849–2874.

Merino, N., Jourdain, N. C., Le Sommer, J., Goosse, H., Mathiot, P., & Durand, G. (2018). Impact of increasing antarctic glacial freshwater release on regional sea-ice cover in the southern ocean. *Ocean Modelling*, *121*, 76–89.

Merino, N., Le Sommer, J., Durand, G., Jourdain, N. C., Madec, G., Mathiot, P., & Tournadre, J. (2016). Antarctic icebergs melt over the southern ocean: Climatology and impact on sea ice. *Ocean Modelling*, *104*, 99–110.

Moorman, R., Morrison, A. K., & McC. Hogg, A. (2020). Thermal responses to antarctic ice shelf melt in an eddy-rich global ocean–sea ice model. *Journal of Climate*, *33*(15), 6599–6620.

Morlighem, M., Rignot, E., Binder, T., Blankenship, D., Drews, R., Eagles, G., … others (2020). Deep glacial troughs and stabilizing ridges unveiled beneath the margins of the antarctic ice sheet. *Nature Geoscience*, *13*(2), 132–137.

Mouginot, J., Rignot, E., & Scheuchl, B. (2014). Sustained increase in ice discharge from the amundsen sea embayment, west antarctica, from 1973 to 2013. *Geophysical Research Letters*, *41*(5), 1576–1584.

Nakayama, Y., Menemenlis, D., Zhang, H., Schodlok, M., & Rignot, E. (2018). Origin of circumpolar deep water intruding onto the amundsen and bellingshausen sea continental shelves. *Nature communications*, *9*(1), 1–9.

Nakayama, Y., Timmermann, R., Rodehacke, C. B., Schröder, M., & Hellmer, H. H. (2014). Modeling the spreading of glacial meltwater from the amundsen and bellingshausen seas. *Geophysical Research Letters*, *41*(22), 7942–7949.

Orsi, A. H., Whitworth III, T., & Nowlin Jr, W. D. (1995). On the meridional extent and fronts of the antarctic circumpolar current. *Deep Sea Research Part I: Oceanographic Research Papers*, *42*(5), 641–673.

Peng, G., Meier, W. N., Scott, D., & Savoie, M. (2013). A long-term and reproducible passive microwave sea ice concentration data record for climate studies and monitoring. *Earth System Science Data*, *5*(2), 311–318.

Pörtner, H., Roberts, D., Masson-Delmotte, V., Zhai, P., Tignor, M., Poloczanska, E., … others (2019). Summary for policymakers. *IPCC special report on the ocean and cryosphere in a changing climate*.

Rignot, E., Jacobs, S., Mouginot, J., & Scheuchl, B. (2013). Ice-shelf melting around antarctica. *Science*, *341*(6143), 266–270.

Rignot, E., Mouginot, J., Scheuchl, B., van den Broeke, M., van Wessem, M. J., & Morlighem, M. (2019). Four decades of antarctic ice sheet mass balance from 1979–2017. *Proceedings of the National Academy of Sciences*, *116*(4), 1095–1103.

Rodriguez, A. R., Mazloff, M. R., & Gille, S. T. (2016). An oceanic heat transport pathway to the amundsen sea embayment. *Journal of Geophysical Research: Oceans*, *121*(5), 3337–3349.

Rosier, S. H., Reese, R., Donges, J. F., De Rydt, J., Gudmundsson, G. H., & Winkelmann, R. (2020). The tipping points and early-warning indicators for pine island glacier, west antarctica. *The Cryosphere Discussions*, 1–23.

Rousset, C., Vancoppenolle, M., Madec, G., Fichefet, T., Flavoni, S., Barthélemy, A., … others (2015). The louvain-la-neuve sea ice model lim3. 6: global and regional capabilities. *Geoscientific Model Development*, *8*(10), 2991–3005.

Spence, P., Holmes, R. M., Hogg, A. M., Griffies, S. M., Stewart, K. D., & England, M. H. (2017). Localized rapid warming of west antarctic subsurface waters by remote winds. *Nature Climate Change*, *7*(8), 595–603.
Steig, E. J., Ding, Q., Battisti, D., & Jenkins, A. (2012). Tropical forcing of circumpolar deep water inflow and outlet glacier thinning in the amundsen sea embayment, west antarctica. *Annals of Glaciology*, *53*(60), 19–28.
Stewart, A. L., & Thompson, A. F. (2015). Eddy-mediated transport of warm circumpolar deep water across the antarctic shelf break. *Geophysical Research Letters*, *42*(2), 432–440.
St-Laurent, P., Klinck, J. M., & Dinniman, M. S. (2013). On the role of coastal troughs in the circulation of warm circumpolar deep water on antarctic shelves. *Journal of Physical Oceanography*, *43*(1), 51–64.
Thoma, M., Jenkins, A., Holland, D., & Jacobs, S. (2008). Modelling circumpolar deep water intrusions on the amundsen sea continental shelf, antarctica. *Geophysical Research Letters*, *35*(18).
Thompson, A. F., Speer, K. G., & Schulze Chretien, L. M. (2020). Genesis of the antarctic slope current in west antarctica. *Geophysical Research Letters*, *47*(16), e2020GL087802.
Thompson, A. F., Stewart, A. L., Spence, P., & Heywood, K. J. (2018). The antarctic slope current in a changing climate. *Reviews of Geophysics*, *56*(4), 741–770.
Uppala, S. M., Kållberg, P., Simmons, A., Andrae, U., Bechtold, V. D. C., Fiorino, M., … others (2005). The era-40 re-analysis. *Quarterly Journal of the Royal Meteorological Society: A journal of the atmospheric sciences, applied meteorology and physical oceanography*, *131*(612), 2961–3012.
Wåhlin, A., Muench, R., Arneborg, L., Björk, G., Ha, H., Lee, S., & Alsén, H. (2012). Some implications of ekman layer dynamics for cross-shelf exchange in the amundsen sea. *Journal of Physical Oceanography*, *42*(9), 1461–1474.
Walker, D. P., Jenkins, A., Assmann, K. M., Shoosmith, D. R., & Brandon, M. A. (2013). Oceanographic observations at the shelf break of the amundsen sea, antarctica. *Journal of Geophysical Research: Oceans*, *118*(6), 2906–2918.
Webber, B. G., Heywood, K. J., Stevens, D. P., & Assmann, K. M. (2019). The impact of overturning and horizontal circulation in pine island trough on ice shelf melt in the eastern amundsen sea. *Journal of Physical Oceanography*, *49*(1), 63–83.
Webber, B. G., Heywood, K. J., Stevens, D. P., Dutrieux, P., Abrahamsen, E. P., Jenkins, A., … Kim, T. W. (2017). Mechanisms driving variability in the ocean forcing of pine island glacier. *Nature communications*, *8*(1), 1–8.